Exchange interaction in the $YbCrBr_9^{3-}$ mixed dimer: The origin of a strong Yb^{3+}-Cr^{3+} exchange anisotropy

V. S. Mironov*
Institute of Crystallography, Russian Academy of Sciences, Leninskii Prosp. 59, 117333 Moscow, Russia

L. F. Chibotaru and A. Ceulemans
Department of Chemistry, Katholieke Universiteit Leuven, Celestijnenlaan 200F, B-3001 Leuven, Belgium
(Received 5 August 2002; published 31 January 2003)

The superexchange interaction between Yb^{3+} and Cr^{3+} ions in the mixed $YbCrBr_9^{3-}$ bioctahedral face-sharing dimer is quantitatively analyzed using a modified kinetic exchange theory, which is adapted to a realistic description of the electronic structure of lanthanide ions in solids. The general procedure of the calculation of the $4f$-$3d$ anisotropic exchange spin Hamiltonian is presented and applied to the $YbCrBr_9^{3-}$ dimer. The spin-Hamiltonian of the Yb^{3+}-Cr^{3+} exchange interaction is found to be extremely anisotropic, $H=J_z S_{\rm Yb}^z S_{\rm Cr}^z + J_\perp (S_{\rm Yb}^x S_{\rm Cr}^x + S_{\rm Yb}^y S_{\rm Cr}^y)$, with the antiferromagnetic J_z and ferromagnetic $J_\perp$ parameters, where $S_{\rm Yb}^\mu$ and $S_{\rm Cr}^\mu$ ($\mu=x,y,z$) are the components of the effective spin $S_{\rm Yb}=\frac{1}{2}$ of the Yb^{3+} ion (corresponding to the ground Γ_6 Kramers doublet) and the true spin $S_{\rm Cr}=\frac{3}{2}$ of the Cr^{3+} ion, respectively. The calculated exchange parameters are quite consistent with the experimental data ($J_z=-5.16\ {\rm cm}^{-1}$ and $J_\perp=+4.19\ {\rm cm}^{-1}$) at reasonable values of the Yb→Cr and Yb←Cr charge transfer energies. The contributions to the J_z and $J_\perp$ exchange parameters from the individual states of the $4f^{12}$-$3d^4$ and $4f^{14}$-$3d^2$ charge transfer configurations are analyzed in detail and general regularities are established. Our results indicate that a very strong $4f$-$3d$ exchange anisotropy can appear even in the absence of the crystal-field anisotropy on the lanthanide ion.

DOI: 10.1103/PhysRevB.67.014424 PACS number(s): 71.70.Gm, 75.30.Et, 76.30.Kg

I. INTRODUCTION

There has been an increasingly intensive research effort in the last decades toward understanding the magnetic properties of lanthanide compounds. The interest to these compounds, and especially to mixed $4f$-$3d$ metal oxides, is receiving renewed attention in connection with the discovery of high-T_c superconductivity and, more recently, of the colossal magnetoresistance.[1] At present, a large variety of insulating lanthanide compounds with different element compositions and various crystal structures are known. Among them the most studied are numerous rare-earth (lanthanide) cuprates (of which $LnBa_2Cu_3O_x$ and Nd_2CuO_4 have attracted a special interest),[2,3] $LnMO_3$ perovskites, such as $NdCrO_3$,[4] $TbMnO_3$,[5] $NdFeO_3$,[6] etc., $Ln_3M_5O_{12}$ garnets,[7] and many other mixed or pure lanthanide compounds.[8,9]

It is commonly recognized that a strong magnetic anisotropy is a general property of the *f*-block element compounds (except those containing $4f^7$ ions, such as Gd^{3+}, Eu^{2+}, or Tb^{4+}). Both single-ion magnetic characteristics and exchange interactions between magnetic centers in lanthanide or actinide compounds are known to be strongly anisotropic.[10–15] Despite extensive and interesting collection of experimental data on magnetic properties of nonmetallic lanthanide compounds, very little is known about specific mechanisms of $4f$-$3d$ or $4f$-$4f$ exchange interactions. In many theoretical approaches, model anisotropic spin Hamiltonians, such as the Ising or *XY* Hamiltonian, are used to describe magnetic properties of lanthanide compounds. However, the microscopic origin of the exchange parameters and their relation to the nature of the magnetic centers, the electronic structure of lanthanide ions, and the specific crystal structure was scarcely analyzed in the literature.[16–19]

In contrast to transition metal ions, exchange interactions between two individual paramagnetic centers *A* and *B*, one or both of which are lanthanide ions, cannot be described in terms of the conventional isotropic Heisenberg Hamiltonian $-J\mathbf{S}_A\mathbf{S}_B$, even to a first approximation. The fundamental reason is that the total spin $\mathbf{S}$ of the $4f^N$ shell of a lanthanide ion is not a good quantum number. This is related to the fact that in lanthanide ions the ratio between the spin-orbit coupling energy ζ and the crystal-field splitting energy Δ is much larger (typically, $\zeta/\Delta>1$) as compared to that in transition metal ions ($\zeta/\Delta=0.01-0.1$ in $3d$ ions). The total spin $\mathbf{S}$ of a transition metal ion is normally a good quantum number, because in most cases the orbital momentum $\mathbf{L}$ is quenched due to a strong crystal-field effect. Therefore, exchange interactions between transition metal ions, with well-separated spin-only ground states, are basically described by the isotropic Heisenberg model with small anisotropic exchange terms appearing due to the spin-orbit coupling

$$H=-J\mathbf{S}_A\mathbf{S}_B+\mathbf{S}_A\mathbf{D}\cdot\mathbf{S}_B+\mathbf{A}[\mathbf{S}_A\times\mathbf{S}_B], \qquad (1)$$

where the second term corresponds to the symmetric anisotropic interaction ($\mathbf{D}$ is a traceless second rank tensor) and the last term is the Dzyaloshinskii-Moriya antisymmetric exchange.[20] The relative magnitude of these anisotropic terms is estimated as $|\mathbf{D}|/J\approx(\zeta/\Delta)^2$ and $|\mathbf{A}|/J\approx\zeta/\Delta$, respectively. For transition metal ions with more than one unpaired electrons ($S>\frac{1}{2}$) some higher powers in spins can also appear.

In lanthanide compounds the situation is quite different. Due to a strong spin-orbit coupling (ζ ranges from 600 to 3000 $\rm cm^{-1}$) combined with a very small crystal-field (CF)

splitting Δ (few hundreds wave numbers), the total orbital momentum $\mathbf{L}$ in lanthanide ions is not quenched since it is coupled to the total spin $\mathbf{S}$ to form the total angular momentum $\mathbf{J}$. The latter is split into CF levels by the ligand surrounding. As a result, neither $\mathbf{L}$ nor $\mathbf{S}$ are no longer good quantum numbers, and the anisotropic terms in the exchange Hamiltonian are no longer small as compared to the isotropic term $-J\mathbf{S}_A\cdot\mathbf{S}_B$.

The magnetic behavior of transition metal and lanthanide compounds with extended magnetic lattices is often very complicated due to cooperative effects making difficult the unambiguous determination of the exchange parameters of the anisotropic spin Hamiltonian (1) from experimental data. Dimers of paramagnetic ions are free of these difficulties and thus are much more favorable for both experimental and theoretical study of exchange interactions.[21] There was a great deal of work on magnetic and optical properties of dimers in solids, mostly on transition metal dimers.[22] Although lanthanide dimers are less studied, some lanthanide-containing exchange pairs were magnetically characterized from optical spectra, electron paramagnetic resonance, and neutron-scattering experiments.[11,23–29]

Exchange interactions in insulating lanthanide compounds, such as those in respective transition metal compounds, can be described in terms of the superexchange model.[30] The underlying mechanism of the magnetic coupling between paramagnetic centers in metal dimers and extended magnetic systems is the kinetic exchange mechanism related to metal-to-metal electron-transfer processes mediated by bridging diamagnetic ligands. Although general principles of the kinetic exchange mechanism are the same for both $3d$ and $4f$ metal ions, specific details of exchange interactions may be however quite different.

This paper deals with the microscopic origin of the exchange interaction between lanthanide and transition metal ions in mixed $4f$-$3d$ dimers. Specifically, we study the mechanism of the kinetic exchange interaction between Yb^{3+} and Cr^{3+} ions in the $YbCrBr_9{}^{3-}$ dimer. This choice has the advantage that there are three structurally related dimers $Cr_2Br_9{}^{3-}$, $YbCrBr_9{}^{3-}$, and $Yb_2Br_9{}^{3-}$, whose magnetic properties have been well characterized. The chromium and ytterbium dimers are contained as individual isolated building blocks in compounds $Cs_3Cr_2Br_9$ (Ref. 31) and $Cs_3Yb_2Br_9$,[32] respectively, while the $YbCrBr_9{}^{3-}$ dimer is obtained by doping Cr^{3+} ions in $Cs_3Yb_2Br_9$ crystals.[26] These dimers consist of two face-sharing $CrBr_6{}^{3-}$ or $YbBr_6{}^{3-}$ octahedra with an approximate D_{3h} or C_{3v} symmetry. Exchange parameters for the Cr^{3+}-Cr^{3+},[33] Yb^{3+}-Yb^{3+},[25] and Yb^{3+}-Cr^{3+} (Ref. 26) pairs were obtained from inelastic neutron scattering experiments. A high local symmetry around the metal ions and their simple electronic configurations ($4f^{13}$ for Yb^{3+} ion and $3d^3$ for Cr^{3+} ion) facilitates considerably the theoretical analysis. The Yb^{3+}-Cr^{3+} exchange interaction in the $YbCrBr_9{}^{3-}$ dimer was found to be extremely anisotropic, $H=-J_zS^z_{Yb}S^z_{Cr}-J_\perp(S^x_{Yb}S^x_{Cr}+S^y_{Yb}S^y_{Cr})$ (where $S_{Yb}=\frac{1}{2}$ and $S_{Cr}=\frac{3}{2}$) with $J_z=-0.64$ meV (-5.16 cm^{-1}) and $J_\perp=+0.52$ meV ($+4.19$ cm^{-1}) (i.e., the exchange parameters J_z and $J_\perp$ have opposite signs). It is also surprising that the exchange interaction between Yb^{3+} ions in the $Yb_2Br_9{}^{3-}$ dimer is isotropic and antiferromagnetic with $J=-2.87$ cm^{-1}.[25] The exchange interaction in the $Cr_2Br_9{}^{3-}$ dimer is antiferromagnetic, $J=-8$ cm^{-1}; it was a subject of extensive experimental and theoretical studies.[22,33,34] Such a different behavior of the magnetic anisotropy in structurally similar $YbCrBr_9{}^{3-}$ and $Yb_2Br_9{}^{3-}$ dimers is therefore very intriguing.

In this paper, the mechanism of the exchange interaction between Yb^{3+} and Cr^{3+} ions in the $YbCrBr_9{}^{3-}$ dimer is analyzed using a modified kinetic exchange theory, which is adapted to a realistic description of a complicated electronic structure of lanthanide ions in solids; the formalism of this approach allows for direct calculations of the parameters of the anisotropic $4f$-$3d$ exchange Hamiltonians.[35] Our primary purpose is, however, to elucidate the origin of a strong Yb^{3+}-Cr^{3+} exchange anisotropy. Although it is commonly believed that the exchange anisotropy is related to the anisotropy of the g tensor of the metal ions, we will show that this is generally not true and a strong exchange anisotropy can appear even if the g tensor of the $4f$ magnetic ions in the exchange pair is isotropic, as is the case for the octahedral ligand surrounding of the Yb^{3+} and Cr^{3+} ions in the $YbCrBr_9{}^{3-}$ dimer.

The paper is arranged as follows. In Sec. II we outline the general theory of the kinetic exchange interaction between $4f$ and $3d$ metal ions. In Sec. III we describe the calculation of the exchange parameters of the spin Hamiltonian (1) for the $YbCrBr_9{}^{3-}$ dimer. In Sec. IV the results of numerical calculations of parameters of the exchange spin Hamiltonian for the Yb^{3+}-Cr^{3+} pair are discussed and the contributions from individual charge-transfer states to the exchange parameters are analyzed in detail. Some general regularities of the $4f$-$3d$ superexchange mechanism are established, which prove to be very helpful in understanding the microscopic origin of a strong exchange anisotropy.

II. THEORY

We describe in this part the theoretical background used for the quantitative description of the $4f$-$3d$ exchange interactions in magnetic insulators following the general concept developed in previous papers.[19,35] Our approach is based on the Anderson's superexchange theory, which is adapted for an adequate description of the electronic structure of lanthanide ions. There are several features of the electronic structure of lanthanide ions, which make the superexchange theory for $4f$ electrons essentially different from that for $3d$ electrons.

(i) In contrast to transition metal ions, in which the magnetic momentum is determined by the total spin only, the magnetic momentum of lanthanide ions is related to the degenerate or quasidegenerate ground state originating from the crystal field splitting of the lowest multiplet. Typically, the ground state of a lanthanide ion is a Kramers doublet corresponding to the effective spin $S=\frac{1}{2}$ with very anisotropic magnetic components. As a result, exchange-split levels of a $4f$-$3d$ dimer cannot be classified according to the total spin as is the case in transition metal dimers.

(ii) The energy spectrum of charge-transfer (CT) states of

a $4f^N$-$3d^M$ dimer is too complicated to be described in terms of a conventional scheme, according to which the CT states are regarded as degenerate and lying at a large energy U above the ground state of the dimer.[30]

(iii) Because of strong electron correlation effects and strong spin-orbit coupling, wave functions of the open $4f^N$ shell are composed of many Slater determinants, both for the ground state and excited CT states. Therefore, electron transfers between metal ions cannot be regarded as transfers between individual $4f$ and $3d$ orbitals of different ions, but they should be regarded as transitions between many-electron states of the system.

In this paper, we concentrate on the microscopic mechanisms of exchange interactions for an isolated lanthanide-transition metal pair ($4f$-$3d$ dimer) rather than for an extended magnetic crystal. We develop the exchange theory in the spirit of the original Anderson approach, but with one important difference. The kinetic exchange theory is developed here in terms of many-electron wave functions constructed from many-electron wave functions of isolated $4f$ and $3d$ metal centers. This approach incorporates a realistic description of the electronic structure of lanthanide ions taking advantage of the well-elaborated parametric approach widely used for the description of the energy level patterns of lanthanide ions in solids.[36–38]

Consider a $4f$-$3d$ exchange-coupled pair AB composed of a lanthanide ion A with the $4f^N$ configuration, a transition metal B with the $3d^M$ configuration, and diamagnetic ligands around each metal center. Some of these ligands bridge the A and B metal centers and mediate exchange interactions between them.

We start from the total electronic Hamiltonian H of the $4f$-$3d$ pair

$$H = H_A + H_B + V, \tag{2}$$

where H_A and H_B are electronic Hamiltonians of the lanthanide and transition metal centers having the $4f^N$ and $3d^M$ basic configurations, respectively, and V incorporates interactions between these centers. Below we specify the structure of these terms in more detail.

A. The Hamiltonian of the $4f^N$ center

The Hamiltonian H_A has the structure

$$H_A = H_0(4f) + H_{\mathrm{CF}}, \tag{3}$$

where $H_0(4f)$ is the free-ion Hamiltonian of the $4f^N$ configuration and H_{CF} is the crystal-field (CF) Hamiltonian. $H_0(4f)$ is often written in the well-elaborated parametric form[36–38]

$$H_0(4f) = \sum_{k=2,4,6} f_k F^k + \sum_i \zeta_{4f} l_i s_i + \alpha L(L+1) + \beta G(G_2) + \gamma G(R_7), \tag{4}$$

which includes the electron repulsion energy, spin-orbit coupling, and the α, β, and γ two-body correction parameters associated to the angular momentum L and to the Casimir operators G for the groups G_2 and R_7, respectively. This Hamiltonian describes the $^{2S+1}L_J$ multiplet structure of the free lanthanide ion, which was analyzed in great details elsewhere.[36–38] Note that $H_0(4f)$ describes the multiplet structure in the true intermediate coupling scheme, not in the simplified Russell-Saunders approach. Under the influence of the CF potential created by the ligand surrounding, $^{2S+1}L_J$ multiplets are split into individual crystal field levels. In many works on the theoretical and optical study of the energy spectra of lanthanide compounds, this splitting is described in terms of the parametric CF Hamiltonian H_{CF}

$$H_{\mathrm{CF}} = \sum_{kq} B_q^k C_q^k, \tag{5}$$

where B_q^k are crystal field parameters associated with spherical tensor operators C_q^k.[36] The H_{CF} Hamiltonian lifts the $2J+1$ degeneracy of the $^{2S+1}L_J$ multiplets with the half-integer total momentum J into doubly degenerated CF states (i.e., Kramers doublets).

Because in the frame of the kinetic exchange theory the $4f$ and $3d$ metal centers in the dimer can interchange one electron, we assume in the following that H_A describes the electronic structure not only for the basic $4f^N$ configuration, but for the charge-transfer configurations $4f^{N-1}$ and $4f^{N+1}$ as well

$$H_A \Psi_k(4f^N) = E_k(4f^N)\Psi_k(4f^N), \tag{6a}$$

$$H_A \Psi_r(4f^{N+1}) = E_r(4f^{N+1})\Psi_r(4f^{N+1}), \tag{6b}$$

$$H_A \Psi_p(4f^{N-1}) = E_p(4f^{N-1})\Psi_p(4f^{N-1}), \tag{6c}$$

where $\Psi_k(4f^N)$, and $\Psi_r(4f^{N+1})$ and $\Psi_p(4f^{N-1})$ are wave functions of the individual CF states of the respective configurations and $E_k(4f^N)$, $E_r(4f^{N+1})$, and $E_p(4f^{N-1})$ are the corresponding CF energies. Although the *f-d* superexchange theory developed in this paper can be applied to various types of the degenerate or pseudodegenerate ground CF state of the f ion (see Sec. V), in this paper we treat with Kramers' lanthanide ions only, i.e., we suppose the number N to be odd, for which the $^{2S+1}L_J$ multiplets with a half-integer moment J are split by the crystal field into Kramers doublets. In particular, the ground state of the lanthanide ion is the $\Psi_0(4f^N; \pm\frac{1}{2})$ Kramers doublet with two components $+\frac{1}{2}$ and $-\frac{1}{2}$ formally corresponding to an effective spin $S=\frac{1}{2}$.

There are two features of the spectrum of $4f^N$ configurations, which should be taken into account for an adequate treatment of the superexchange interactions involving lanthanide ions. First, the total number of states involved can be very large, 91 ($4f^2$,$4f^{12}$) 364 ($4f^3$,$4f^{11}$), 1001 ($4f^4$,$4f^{10}$), 2002 ($4f^5$,$4f^9$), 3003 ($4f^6$,$4f^8$), and 3432 ($4f^7$). Second, the total energy extension $\Delta E(4f^N)$ of the spectrum of $4f^N$ configurations is usually large ranging from 6 eV ($4f^2$) to about 20 eV ($4f^7$-$4f^{10}$) (see Table I). Typically, the energy distance between the $^{2S+1}L_J$ multiplets is of the order of few thousands cm^{-1}, the CF splitting is of order of several hundreds cm^{-1}, and the energy gap between the ground and first excited CF state varies from few cm^{-1} to several hundreds cm^{-1}, depending on the nature of the lanthanide ion and the

TABLE I. The total energy range of $4f^N$ configurations of lanthanide ions $[\Delta E(4f^N)]$ and $3d^M$ configurations of octahedrally coordinated transition metal ions $[\Delta E(3d^M)]$.

$4f^N$ configuration		$3d^M$ configuration	
$4f^N$	$\Delta E(4f^N)$, eV[a]	$3d^M$	$\Delta E(3d^M)$, eV[b]
$4f^1$	0.3	$3d^1$	1.9
$4f^2$	5.8	$3d^2$	6.9
$4f^3$	8.4	$3d^3$	8.2
$4f^4$	15.7	$3d^4$	11.2
$4f^5$	16.1	$3d^5$	10.1
$4f^6$	22.1	$3d^6$	11.5
$4f^7$	22.5	$3d^7$	7.5
$4f^8$	24.0	$3d^8$	7.5
$4f^9$	18.3	$3d^9$	1.9
$4f^{10}$	20.0		
$4f^{11}$	12.1		
$4f^{12}$	9.8		
$4f^{13}$	1.2		

[a]Calculated for lanthanide ions with the free-ion parameters of Ln^{3+} ion (Ref. 41).

[b]Calculated with the $B=700$, $C=3000\ \mathrm{cm}^{-1}$ Racah parameters and $10Dq=15\,000\ \mathrm{cm}^{-1}$.

type of ligands surrounding.[37] It is also important to stress that the wave functions $\Psi_0(4f^N;\pm\frac{1}{2})$ of the ground Kramers doublet of the lanthanide ion are represented by a sum of many determinants, and they cannot be reduced to a single Slater determinant (see below). This makes inadequate the widely used approach based on one-configuration approximation for the wave functions of the ground magnetic state.

B. The Hamiltonian of the $3d^M$ center

Similar relations are valid for the transition metal center B of the dimer. The Hamiltonian of an isolated $3d$ center is represented by

$$H_B=H_0(3d)+H_{\mathrm{CF}}, \tag{7}$$

where $H_0(3d)$ describes Coulomb interactions between $3d$ electrons and H_{CF} corresponds to the CF potential. The wave functions $\Phi_i(3d^M;SM_s)$ and CF energies $E_i(3d^M)$ of the basic $3d^N$ configuration are defined by

$$H_B\Phi_i(3d^M;SM_s)=E_i(3d^M)\Phi_i(3d^M;SM_s). \tag{8}$$

Since we do not take into account the spin-orbit interaction on the transition metal ion, each CF state $\Phi_i(3d^M;S,M_s)$ is characterized by the definite total spin S_i and its projection M_s, which are good quantum numbers. Note that the index i refers to the orbital part of the wave function and the total spin S is therefore a function of i. We suppose that the $\Phi_0(3d^M;SM_s)$ ground state is orbitally nondegenerate and has a nonzero spin S. Again, the Hamiltonian H_B is also defined for the $3d^{M+1}$ and $3d^{M-1}$ CT configurations

$$H_B\Phi_q(3d^{M+1};S'M')=E_q(3d^{M+1})\Phi_q(3d^{M+1};S'M'), \tag{9a}$$

$$H_B\Phi_s(3d^{M-1};S'M')=E_s(3d^{M-1})\Phi_s(3d^{M-1};S'M'). \tag{9b}$$

For the crystal field of the cubic symmetry, the energy level scheme of $3d^M$ configurations is described by the Tanabe-Sugano diagrams.[39,40] In the general case, when the system has a low symmetry or no symmetry at all, the energy spectrum should be obtained from the exact diagonalization of H_B. Note that in the following no symmetry in the $4f$-$3d$ dimer AB is supposed.

C. The unperturbed Hamiltonian and the charge-transfer energy spectrum of a $4f^N$-$3d^M$ dimer

In the absence of interactions between $4f$ and $3d$ ions, the wave functions of the $4f$-$3d$ dimer are described by the one-center Hamiltonians H_A+H_B. Their eigenvectors $\Xi_{kl}(AB;SM_s)$ are written as direct antisymmetrized products of the corresponding wave functions of centers A and B. For the basic $4f^N$-$3d^M$ configuration of the dimer we have

$$\Xi_{kl}(AB;SM_s)=\Psi_k(4f^N)\otimes\Phi_l(3d^M;SM_s), \tag{10}$$

where $\otimes$ stands for the antisymmetrized product. In particular, the ground level of the unperturbed dimer is $2S(S+1)$-fold degenerate and is represented by the set of the $|\pm 1/2,M_s\rangle$ wave functions

$$|\pm 1/2,M_s\rangle=\Psi_0(4f^N;\pm 1/2)\otimes\Phi_0(3d^M;SM_s). \tag{11}$$

The eigenenergies of H_A+H_B are sums of separate one-center contributions $E_k(4f^N)+E_l(3d^M)$. H_A+H_B describes also the CT configurations. The eigenfunctions $\Xi_{pq}(A\rightarrow B;S'M')$ and $\Xi_{rs}(A\leftarrow B;S'M')$ corresponding to the CT states, $4f^{N-1}$-$3d^{M+1}$ and $4f^{N+1}$-$3d^{M-1}$, are defined by

$$\Xi_{pq}(A\rightarrow B;S'M')=\Psi_p(4f^{N-1})\otimes\Phi_q(3d^{M+1};S'M'), \tag{12a}$$

$$\Xi_{rs}(A\leftarrow B;S'M')=\Psi_r(4f^{N+1})\otimes\Phi_s(3d^{M-1};S'M'). \tag{12b}$$

The corresponding eigenenergies are sums of the single-ion energies of the, respective $4f^{N\pm1}$ and $3d^{M\pm1}$ configuration plus the CT energy gap $U_0(A\rightarrow B)$ or $U_0(A\leftarrow B)$, which is the difference between the energy of the ground states of the basic $4f^N$-$3d^M$ and the CT configuration $4f^{N-1}$-$3d^{M+1}$ ($4f^{N+1}$-$3d^{M-1}$) CT configuration

$$E_{pq}(A\rightarrow B)=U_0(A\rightarrow B)+E_p(4f^{N-1})+E_q(3d^{M+1}), \tag{13a}$$

$$E_{rs}(A\rightarrow B)=U_0(A\rightarrow B)+E_r(4f^{N+1})+E_s(3d^{M-1}). \tag{13b}$$

For the $4f$-$3d$ dimer with noninteracting centers A and B, these energies are defined by intracenter interactions only; they also incorporate the energy difference between $4f$ and $3d$ orbitals and the electron repulsion energy between $4f$ or $3d$ electrons on the respective metal centers. For a heterometallic AB dimer, the $U_0(A\rightarrow B)$ or $U_0(A\leftarrow B)$ CT energy gaps can be different. In many treatments of superexchange, $E_{pq}(A\rightarrow B)$ and $E_{rs}(A\leftarrow B)$ quantities are often reduced to

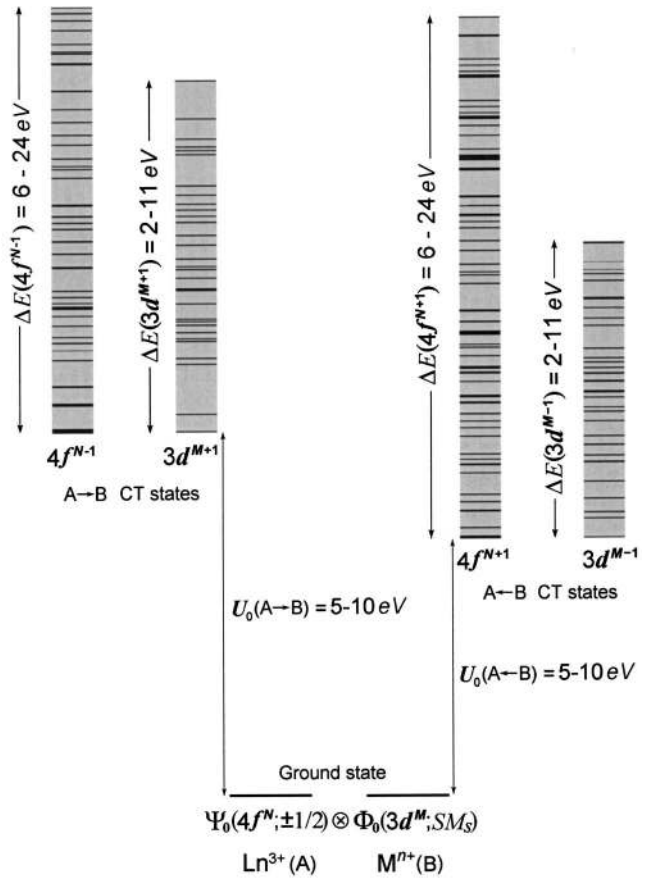

FIG. 1. The energy band structure of the CT configurations of a $4f^N$-$3d^M$ exchange dimer. The $\Psi_0(4f^N;\pm 1/2)\otimes\Phi_0(3d^M;SM_s)$ ground state of the $4f^N$-$3d^M$ basic configuration is separated from the ground state of the $4f^{N-1}$-$3d^{M+1}$ and $4f^{N+1}$-$3d^{M-1}$ CT configurations by the energy gap $U_0(A\rightarrow B)$ and $U_0(A\leftarrow B)$, respectively. The total energy extension of the CT configurations is given by the sum $\Delta E(4f^{N-1})+\Delta E(3d^{M+1})$ or $\Delta E(4f^{N+1})+\Delta E(3d^{M-1})$ and may reach a value of 35 eV being far beyond the typical CT energy gap of 5–10 eV.

the single Hubbard energy U. In fact, for $4f$-$3d$ dimers this simple superexchange model is far from being realistic. Indeed, since the total energy range of the $4f^{N\pm 1}$ and $3d^{M\pm 1}$ configurations [$\Delta E(4f^{N\pm 1})$ and $\Delta E(3d^{M\pm 1})$] is very large [up to 24 eV for $\Delta E(4f^{N\pm 1})$ and 11 eV for $\Delta E(3d^{M\pm 1})$, see Table I], the total width of the CT band of a $4f$-$3d$ dimer is normally well above 10 eV and can reach a value of 35 eV, which is much larger than the typical metal-to-metal CT energy U ranging within 5–10 eV.[30] This is illustrated by Fig. 1. Therefore, the energies of individual CT states of the $4f$-$3d$ dimer should be taken into account explicitly. As shown in Sec. IV, this is very important in order to obtain a correct balance between contributions of these states to the exchange parameters.

Now we take into account the interaction V between the $4f$ and $3d$ centers and define the unperturbed Hamiltonian of the dimer AB. The interaction V can be written as

$$V = V_{AB} + H_{AB}, \tag{14}$$

where V_{AB} incorporates those interactions between $4f$ and $3d$ metal centers, which do not mix the states of the $4f^N$-$3d^M$ basic configuration with the states of $4f^{N-1}$-$3d^{M+1}$ or $4f^{N+1}$-$3d^{M-1}$ CT configurations. H_{AB} describes electron transfers between A and B metal centers. V_{AB} is mainly contributed by the intercenter Coulomb interactions between $4f$ and $3d$ electrons, $V_{\mathrm{Coul}}(AB)$. Indeed, $\langle \Xi_{kl}(AB;SM_s)|V_{\mathrm{Coul}}(AB)|\Xi_{pq}(A\rightarrow B;S'M')\rangle$ matrix elements are negligibly small because of a very small overlap of $4f$ and $3d$ orbitals centered on different metal ions. In addition, $V_{\mathrm{Coul}}(AB)$ acts diagonally in the space of wave functions of the $4f^N$-$3d^M$ basic configuration and causes some splitting of spin levels due to the direct (potential) $4f$-$3d$ exchange interaction J_{fd}. As in transition metal exchange dimers, the latter is assumed to be small (actually, the direct exchange interaction in $4f$-$3d$ dimers seems to be even less important than in $3d$-$3d$ dimers because of a strongly localized character of $4f$ states). Hereafter we concentrate on the kinetic exchange contributions only.

The unperturbed Hamiltonian of the $4f$-$3d$ dimer is formally defined as

$$H_0 = H_A + H_B + V_{AB}. \tag{15}$$

The Hamiltonian H_0 is defined in the extended basis set, which involves the wave functions (10) of the $4f^N$-$3d^M$ configuration and the wave functions (12) of the $4f^{N-1}$-$3d^{M+1}$ and $4f^{N+1}$-$3d^{M-1}$ configurations. It incorporates all intracenter and intercenter interactions, which do not mix the AB states with the $A\rightarrow B$ and $A\leftarrow B$ CT states (12). In our approach, H_0 is not expressed explicitly via specific one-and two-electron operators, but it is defined by the full set of its eigenvectors and eigenenergies. Consider first the eigenvectors of H_0. Generally, they should not differ much from the eigenvectors (10) and (12) of the H_A+H_B Hamiltonian, describing the dimer with the noninteracting centers A and B. Indeed, the wave functions of $4f$ or $3d$ metal ions are formed mainly by the intraionic interactions and by the interactions with the nearest ligands; interactions with more distant atoms, including the neighboring paramagnetic metal atoms, have a considerably smaller influence on the single-ion wave functions (we do not consider here the formation of metal-metal bonds). In other words, the wave functions of the localized $4f^N$ or $3d^M$ shell of the given metal ion defined by Eqs. (6), (8), and (9) are essentially the same irrespective of the presence or absence of other paramagnetic metal ions outside the nearest coordination sphere. In particular, this is reflected in the fact that the energy positions of lines in optical spectra of lanthanide and transition metal ions diluted in insulating solids do not vary much with increasing the concentration. This is also evidenced from numerous data on magnetic and optical properties of individual binuclear metal complexes, which show that the line energies (but not optical intensities) in their optical spectra are very close to those of the corresponding isolated metal ions in the similar ligand coordination.[22,37,40] Therefore, it is a good approximation to assume that the eigenvectors of the Hamiltonian H_0 coincide with those of the H_A+H_B, which are given by the direct products of the one-center wave functions (10) and (12).

The eigenenergies of H_0 differ from those of H_A+H_B due to the intercenter interaction V_{AB}. However, since the intercenter interactions are considerably weaker than the intracenter interactions, the energy spectrum of H_0 should be close to the spectrum of the H_A+H_B Hamiltonian (13). For the basic configuration $4f^N$-$3d^M$ the intercenter Coulomb interaction is manifested as electric multipolar interaction between $4f$ and $3d$ electrons, which is considerably smaller than the intraionic Coulomb and CF interactions and thus can be omitted. For the $4f^{N-1}$-$3d^{M+1}$ configuration the intercenter Coulomb interaction is more pronounced since now it describes the direct interaction between the hole in the $4f^{N-1}$ shell and the extra electron in the $3d^{M+1}$ shell (or vice versa for the $4f^{N+1}$-$3d^{M-1}$ CT configuration). This energy is of the order of 1–2 eV, which is still small as compared to the $A\rightarrow B$ CT energy $U_0(A\rightarrow B)=5-10$ eV. It is important that this interaction is mainly reduced to the point-charge Coulomb interaction, which shifts the energy positions of CT states by the same value and thus does not influence much their order. This implies that the V_{AB} interaction for CT states can be absorbed by the CT energy gap $U_0(A\rightarrow B)$ or $U_0(A\leftarrow B)$.

Thus, the unperturbed Hamiltonian H_0 of the $4f$-$3d$ dimer is as an operator with eigenvectors (10) and (12) and the corresponding energies (13), in which the $U_0(A\rightarrow B)$ and $U_0(A\leftarrow B)$ CT energy gaps incorporate the energy of the direct intercenter $4f$-$3d$ interactions. This definition of the unperturbed Hamiltonian is convenient for a model description of exchange dimers, since explicit expression of effective interactions via specific one-and two-electron operators may be uncertain.

D. The perturbation Hamiltonian

The perturbation Hamiltonian H_{AB} describes $4f\rightarrow 3d$ and $4f\leftarrow 3d$ electrons transfers mixing the ground and CT configurations. It represents the sum of one-electron operators $h(i)$

$$H_{AB}=\sum_i h(i). \tag{16}$$

Each operator $h(i)$ is defined by a 7×5 matrix with the elements $t(4f_i\text{-}3d_j)\equiv\langle 4f_i|h|3d_j)\rangle$ (hereafter abbreviated as t_{ij}) connecting seven $4f_i$ orbitals centered on the lanthanide ion A with five $3d_j$ orbitals centered on the transition-metal ion B; these quantities are called transfer (hopping) integrals. They describe the indirect coupling between the lanthanide $4f$ and $3d$ metal atomic orbitals via the intermediate s and p ligands orbitals (see Sec. III).

In the second-quantized technique H_{AB} is written in the usual form

$$H_{AB}=\sum_{ij} t_{ij}a_i^+ b_j+\text{H.c.}, \tag{17}$$

where a_i^+ and b_j are second quantization operators corresponding to the $4f_i$ and $3d_j$ orbitals. In our approach, H_{AB} is represented by the full set of the matrix elements $\langle\Xi_{kl}(AB;SM_s)|H_{AB}|\Xi_{pq}(A\rightarrow B;S'M')\rangle$ and $\langle\Xi_{kl}(AB;SM_s)|H_{AB}|\Xi_{rs}(A\leftarrow B;S'M')\rangle$ connecting the AB states with the $A\rightarrow B$ or $A\leftarrow B$ CT states. These matrix elements can be directly expressed via the $t(4f_i\text{-}3d_j)$ transfer integrals. Details of these calculations are given in the Appendix A.

E. The effective exchange Hamiltonian H_{eff} of the $4f^N$-$3d^M$ metal dimer

Now we derive the effective exchange Hamiltonian H_{eff} of the $4f^N$-$3d^M$ dimer. By definition, H_{eff} acts in the space of the $2(2S+1)$-fold degenerate ground level of the unperturbed Hamiltonian H_0, which is spanned by the set of $|m,M_s\rangle=\Psi_0(4f^N;m)\otimes\Phi_0(3d^N;SM_s)$ wave functions, where $m=+\frac{1}{2},-\frac{1}{2}$ stands for the components of the ground Kramers doublet of the lanthanide ion and $M_s=S,S-1,...,-S$ is the projection of the total spin S of the ground level of the transition metal center B. H_{eff} is defined by the set of matrix elements

$$\langle m,M_s|H_{\text{eff}}|m',M_s'\rangle. \tag{18}$$

Since the degeneracy of the ground manifold is of a spin nature, matrix elements of H_{eff} can be directly associated with the matrix elements of a conventional exchange spin Hamiltonian written in terms of products of operators S_A^x, S_A^y, and S_A^z of the effective spin $\frac{1}{2}$ of the lanthanide ion A and the S_B^z, S_B^+, and S_B^- operators of the true spin S_B of the transition metal ion B. These operators obey the following equations:

$$S_A^z\Psi_0(4f^N;m)=m\Psi_0(4f^N;m), \tag{19a}$$

$$S_A^x\Psi_0(4f^N;m)=\frac{1}{2}\Psi_0(4f^N;-m), \tag{19b}$$

$$S_A^y\Psi_0(4f^N;m)=im\Psi_0(4f^N;-m), \tag{19c}$$

$$S_B^z\Phi_0(3d^M;SM_s)=M_s\Phi_0(3d^M;SM_s), \tag{19d}$$

$$S_B^+\Phi_0(3d^M;SM_s)=\sqrt{S(S+1)-M_s(M_s+1)}\Phi_0\times(3d^M;SM_s+1), \tag{19e}$$

$$S_B^-\Phi_0(3d^M;SM_s)=\sqrt{S(S+1)-M_s(M_s-1)}\Phi_0\times(3d^M;SM_s-1). \tag{19f}$$

The effective Hamiltonian H_{eff} is obtained by the projection of the total Hamiltonian $H=H_A+H_B+V_{AB}+H_{AB}$ into the space of states $|m,M_s\rangle$ from the ground manifold. To this end we define the projection operators $\mathbf{P}_0$ and $\mathbf{P}_i$ for the ground (AB) and excited CT ($A\rightarrow B$ and $A\leftarrow B$) manifolds

$$\mathbf{P}_0=\sum_{n_0}|n_0\rangle\langle n_0|,\quad \mathbf{P}_i=|n_i\rangle\langle n_i|, \tag{20}$$

where n_0 runs over the $|m,M_s\rangle=\Psi_0(4f^N;m)\otimes\Phi_0(3d^N;SM_s)$ states of the $2(2S+1)$-fold degenerate ground level, and n_i runs over spin-degenerate CT states

$\Xi_{pq}(A\rightarrow B;S'M')=\Psi_p(4f^{N-1})\otimes\Phi_q(3d^{M+1};S'M')$ and $\Xi_{rs}(A\leftarrow B;S'M')=\Psi_r(4f^{N+1})\otimes\Phi_s(3d^{M-1};S'M')$ with the composite indices pq and rs, respectively. In the second order after H_{AB} we obtain for $H_{\rm eff}$

$$H_{\rm eff}=\sum_{i\neq 0}\frac{\mathbf{P}_0H_{AB}\mathbf{P}_iH_{AB}\mathbf{P}_0}{E_0-E_i}. \tag{21}$$

The matrix elements of $H_{\rm eff}$ are given by

$$\langle m,M_s|H_{\rm eff}|m',M_s'\rangle=-\sum_{pq;M'}\frac{\langle m,M_s|H_{AB}|\Xi_{pq}(A\rightarrow B;S'M')\rangle\langle\Xi_{pq}(A\rightarrow B;S'M'|H_{AB}|m',M_s'\rangle}{U_0(A\rightarrow B)+E_p(4f^{N-1})+E_q(3d^{M+1})}$$
$$-\sum_{rs;M'}\frac{\langle m,M_s|H_{AB}|\Xi_{rs}(A\leftarrow B;S'M')\rangle\langle\Xi_{rs}(A\leftarrow B;S'M')|H_{AB}|m',M_s'\rangle}{U_0(A\leftarrow B)+E_r(4f^{N+1})+E_s(3d^{M-1})}. \tag{22}$$

Note that the S_A^η ($\eta=x,y,z$) operators refer to the effective spin $\mathbf{S}_A$ of the lanthanide ion, not to the operators of the magnetic momentum μ_A. They are related to each other via the g-tensor of the ground Kramers doublet of the lanthanide ions, which might be very anisotropic. In the general case, the relationship between $\mathbf{S}_A$ and μ_A is rather complicated, and should be analyzed separately for a specific $4f$-$3d$ dimer. Below we deal with a model $YbCrBr_9^{3-}$ dimer in which the $YbBr_6^{3-}$ coordination polyhedron is assumed to be a regular octahedron. In this case the g tensor of the ground Kramers' doublet of the Yb^{3+} ion is isotropic and thus the effective spin operator $\mathbf{S}_A$ is simply proportional to the magnetic momentum operator μ_A. This will be analyzed in more detail in Sec. III.

Because analytical calculations using Eq. (22) are hardly possible even for simple $4f$-$3d$ dimers, a special computer program for numerical calculations of the spin Hamiltonian exchange parameters was designed. Here we give a brief outline of this program.

There are three groups of input parameters in the program. The first group involves parameters for the lanthanide center A, the free-ion parameters of the lanthanide ion (the electron repulsion parameters F^2, F^4, and F^6, spin-orbit coupling constant ζ_{4f} for $4f$ electrons, and the Trees two-body correction parameters α, β, and γ, Eq. (4), and the full set of the B_q^k parameters (a total of 27 CF parameters) involved in the model CF Hamiltonian, Eq. (5). The second group involves parameters for the transition metal center, the B and C Racah parameters and the set of CF parameters for $3d$ electrons, which are defined as a 5×5 real matrix composed of $\langle 3d_i|H_{\rm CF}|3d_j\rangle$ matrix elements for d orbitals of the cubic basis set. The third group contains parameters describing the interaction between $4f$ and $3d$ centers, the $U_0(A\rightarrow B)$, and $U_0(A\leftarrow B)$ CT energy gaps and the full set of $t(4f_i$-$3d_j)$ transfer integrals (the latter are input as a 7×5 complex matrix).

The program works as follows. First, the single-center Hamiltonians H_A and H_B are diagonalized and the wave functions and energies of the $4f^N$, $4f^{N\pm1}$ and $3d^M$, $3d^{M\pm1}$ configurations are obtained. Then the two-center wave functions are formed and the matrix elements $\langle\Xi_{kl}(AB;SM_s)|H_{AB}|\Xi_{pq}(A\rightarrow B;S'M')\rangle$ and $\langle\Xi_{kl}(AB;SM_s)|H_{AB}|\Xi_{rs}(A\leftarrow B;S'M')\rangle$ between the ground state and excited CT states are calculated. At the last step, the matrix elements $\langle m,M_s|H_{\rm eff}|m',M_s'\rangle$ of the effective exchange Hamiltonian are calculated using Eq. (22), which can be then directly used to find the exchange parameters of the anisotropic $4f$-$3d$ spin Hamiltonian. The program is designed for the general case: it can be used for dimers with each combination of the Kramers lanthanide ion and the paramagnetic transition metal ion; no symmetry is supposed. Below this program is applied to the spin Hamiltonian calculations for the $YbCrBr_9^{3-}$ dimer.

III. SUPEREXCHANGE INTERACTION IN THE $YbCrBr_9^{3-}$ DIMER: THE PARAMETERS OF THE THEORY

The described computational approach to the $4f$-$3d$ superexchange is now applied to the analysis of the exchange interaction between Yb^{3+} and Cr^{3+} ions in the $YbCrBr_9^{3-}$ dimer (a $4f^{13}$-$3d^3$ pair). Our main goal is to elucidate the origin of the strong exchange anisotropy and, particularly, the origin of opposite sign of the J_z and $J_\perp$ exchange parameters for the $YbCrBr_9^{3-}$ dimer. To this end, we use an idealized structural model of the $YbCrBr_9^{3-}$ dimer and we apply a number of approximations. In this section, the necessary parameters of the kinetic exchange theory are determined and the $t(4f_i$-$3d_j)$ transfer integrals between magnetic orbitals in the $YbCrBr_9^{3-}$ dimer are calculated.

A. The model structure of the $YbCrBr_9^{3-}$ dimer and the parameters of the unperturbed Hamiltonian of the Yb^{3+}-Cr^{3+} pair

The $YbCrBr_9^{3-}$ dimers are formed in the $Cs_3Yb_{1.8}Cr_{0.2}Br_9$ crystals, which is obtained by doping $Cs_3Yb_2Br_9$ host compound with 10% of Cr^{3+} ions.[26] The crystal structure of the host compound contains $Yb_2Br_9^{3-}$ dimers as building blocks consisting of two face-sharing $YbBr_6^{3-}$ octahedra. Mixed $YbCrBr_9^{3-}$ dimers (Fig. 2) are formed due to the statistical substitution of Cr^{3+} ions for Yb^{3+} ions. In the parent $Yb_2Br_9^{3-}$ dimer the $YbBr_6^{3-}$ octahedra are somewhat distorted, the terminal Yb-Br bonds being shorter by about 0.2 Å than the bridging bonds.[32] The approximate symmetry of $Yb_2Br_9^{3-}$ is close to D_{3d} point

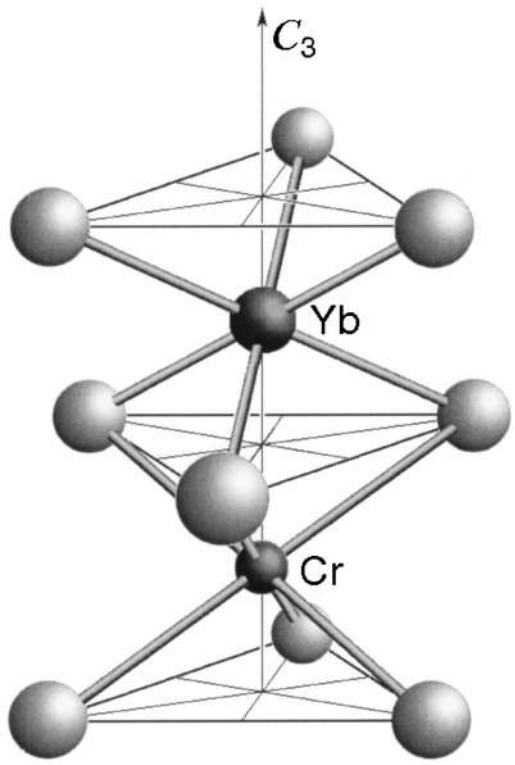

FIG. 2. The structure of the $YbCrBr_9^{3-}$ mixed dimer. Nine bromine atoms are shown as light gray balls. The $YbBr_6$ and $CrBr_6$ polyhedra are assumed to be regular octahedra with the same metal-ligands distances. The dimer has the C_{3v} symmetry with the C_3 rotation axis passing through the Yb and Cr atoms.

group, the true symmetry is C_3. The bioctahedral face-sharing $Cr_2Br_9^{3-}$ dimers in $Cs_3Cr_2Br_9$ have a very similar structure but with shorter metal-ligand distances.[31]

Below we use an idealized structural model for the $YbCrBr_9^{3-}$ mixed dimer, in which both $YbBr_6^{3-}$ and $CrBr_6^{3-}$ units are assumed to be regular octahedra with the same Yb-Br and Cr-Br distances. The use of this approximation makes sense not only for simplicity, but allows to separate the $4f$-$3d$ exchange anisotropy itself from the single-ion anisotropy, which vanishes in the octahedral symmetry of the ligand surrounding. However, in calculating $t(4f_i\text{-}3d_j)$ transfer integrals we will use the actual metal-bromine distances proper to the parent $Cr_2Br_9^{3-}$ and $Yb_2Br_9^{3-}$ dimers.[31,32]

Since the ground $4f^{13}$ configuration of Yb^{3+} corresponds to a single hole, only the spin-orbit coupling constant is involved among the free-ion parameters ($\zeta_{4f}=2900\ \mathrm{cm}^{-1}$). However, for the $4f^{12}$ CT configuration all free-ion parameters of the $H_0(4f)$ Hamiltonian, Eq. (4), should be involved. We use here the parameters of the isoelectronic Tm^{3+} ion [$F^2=103886$, $F^4=77024$, $F^6=57448$, $\zeta_{4f}=2629$, $\alpha=14.677$, $\beta=-631.79\ \mathrm{cm}^{-1}$, and $\gamma=0$ (Ref. 41)]. The set of B_q^k cubic CF parameters corresponds to a trigonal quantization axis C_3 and is chosen to match the CF splitting energy of the ground $^2F_{7/2}$ multiplet of Yb^{3+} ion in $Cs_3Yb_2Br_9$ (about $450\ \mathrm{cm}^{-1}$).[42]

The CF splitting of $3d$ levels in Cr^{3+} ion in the octahedral ligand field is described by the conventional $10Dq$ parameter, which is set to $13\,000\ \mathrm{cm}^{-1}$ (this value is observed in many compounds containing the $CrBr_6^{3-}$ complex anion[40]). The corresponding cubic CF potential is defined for the trigonal quantization axis z. We use $B=700$ and $C=3000\ \mathrm{cm}^{-1}$ Racah parameters which are typical of many six-coordinated pseudo-octahedral trivalent chromium compounds.[40]

The situation with the CT energies is more uncertain. In symmetric dimers with equivalent metal centers, the CT energy gap for the direct ($A\rightarrow B$) and back ($A\leftarrow B$) electrons transfers are equal and can be set to the conventional metal-to-metal energy $U_0(A\rightarrow B)=U_0(A\leftarrow B)\equiv U$, which typically ranges from 5 to 10 eV.[30] In heterometallic pairs, and particularly in $4f$-$3d$, the $U_0(A\rightarrow B)$ and $U_0(A\leftarrow B)$ CT energies are expected to be different due to the differences in the orbital energies and electron repulsion parameters for $4f$ and $3d$ electrons. Due to these uncertainties, below $U_0(A\rightarrow B)$ and $U_0(A\leftarrow B)$ are assumed to be variable parameters each ranging independently from 5 to 12 eV. However, a rough estimate of CT energies can be obtained from electrochemical arguments for Yb^{3+} and Cr^{3+} ions. Since CT energies are related to the loss or gain of an electron by metal ions in a condensed medium, they can be correlated with the difference of the corresponding standard redox potentials of Yb^{3+} and Cr^{3+} ions in aqueous solutions $U_0(A\rightarrow B)\propto E^0(Yb^{4+}/Yb^{3+})-E^0(Cr^{2+}/Cr^{3+})$ and $U_0(A\leftarrow B)\propto E^0(Cr^{4+}/Cr^{3+})-E^0(Yb^{2+}/Yb^{3+})$. Except for $E^0(Yb^{4+}/Yb^{3+})$, these data are available from the literature, $E^0(Yb^{2+}/Yb^{3+})=-1.05$ V, $E^0(Cr^{2+}/Cr^{3+})=-0.424$ V, $E^0(Cr^{4+}/Cr^{3+})=+2.10$ V.[43] Since $E^0(Nd^{4+}/Nd^{3+})=+4.9$ and $E^0(Dy^{4+}/Dy^{3+})=+5.7$ V are known,[43] the redox potential $E^0(Yb^{4+}/Yb^{3+})$ is expected to be very high; approximately, it can set to that of the neighboring Dy^{3+} ion $E^0(Yb^{4+}/Yb^{3+})=+5.7$ V. Thus we obtain $[E^0(Yb^{4+}/Yb^{3+})-E^0(Cr^{2+}/Cr^{3+})]/[E^0(Cr^{4+}/Cr^{3+})-E^0(Yb^{2+}/Yb^{3+})]\approx 2$. Therefore, $U_0(A\rightarrow B)$ is expected to be nearly twice as larger as $U_0(A\leftarrow B)$. Setting the larger CT energy to 10 eV, the upper value of the Hubbard energy,[30] we estimate $U_0(A\rightarrow B)=10$ and $U_0(A\leftarrow B)=5$ eV; these values can be used as a reference in calculations for the $YbCrBr_9^{3-}$ dimer. Below we will show that the exchange parameters calculated at these CT energies do really correspond to the best agreement with the experimental data.

B. $t(4f_i\text{-}3d_j)$ transfer integrals

The transfer integrals $t_{ij}=t(4f_i\text{-}3d_j)$ describing the effective one-electron transfers between ytterbium $4f_i$ and chromium $3d_j$ orbitals in the $YbCrBr_9^{3-}$ dimer, are key parameters of the theory. To calculate the full set of 35 transfer integrals in the model $YbCrBr_9^{3-}$ dimer, we use the conventional second-order perturbation expression corresponding to the case of weak metal-ligand covalence on both the metal sites of the dimer

$$t(4f_i\text{-}3d_j)=-\sum_{L_n}\sum_{\chi_k(L_n)}\frac{\langle 4f_i|h|\chi_k(L_n)\rangle\langle\chi_k(L_n)|h|3d_j\rangle}{E[\chi_k(L_n)\rightarrow fd]}, \tag{23}$$

where the first sum runs over the tree bridging bromide ligands L_n and the second sum runs over the $4s$ and $4p$ orbitals $\chi_k(L_n)$ of these ligands. Matrix elements of the Fock operator h are resonance integrals connecting $4f_i$ or $3d_j$ orbitals of the metal ions and $\chi_k(L_n)$ orbitals of the bridging ligand L_n. The energy denominator is a weighted ligand-metal charge-transfer energy, which is given by

$$\frac{1}{E[\chi_k(L_n \rightarrow fd)]} = \frac{1}{2}\left(\frac{1}{E(4f) - E[(\chi_k(L_n))]} + \frac{1}{E(3d) - E[\chi_k(L_n)]} \right), \qquad (24)$$

where $E(\chi_k)$, $E(4f)$, and $E(3d)$ are the corresponding orbital energies. In our calculations, the $t(4f_i\text{-}3d_j)$ transfer integrals are defined in the basis set of $4f_i$ and $3d_j$ orbitals with the definite projection of the orbital momentum on the C_3 quantization axis z (Fig. 2). The indices i and j stand for the projection of the orbital momentum of $4f$ and $3d$ electrons, respectively.

In the idealized $YbCrBr_9^{3-}$ dimer, the resonance integrals entering Eq. (23) can be expressed analytically via four parameters $\sigma(fp)$, $\pi(fp)$, $\sigma(dp)$, and $\pi(dp)$, corresponding to the resonance integrals defined with respect to the Yb-Br or Cr-Br bond $\sigma(fp) = \langle 4f_0|h|4p_0\rangle$, $\pi(fp) = \langle 4f_{\pm 1}|h|4p_{\pm 1}\rangle$, $\sigma(dp) = \langle 3d_0|h|4p_0\rangle$, and $\pi(dp) = \langle 3d_{\pm 1}|h|4p_{\pm 1}\rangle$, where $4f_k$, $3d_k$ are metal and $4p_k$ are bromine orbitals with the projection of the orbital momentum on the metal-ligand axis ($k = 0, \pm 1$). For each of three Yb-Br-Cr bridges, the products $\langle 4f_i|h|4p_k\rangle\langle 4p_k|h|3d_j\rangle$ in the nominator of Eq. (23) can be written as linear combinations of binary products of the $\sigma(fp)$, $\pi(fp)$, $\sigma(dp)$, and $\pi(dp)$ parameters. The coefficients in these combinations correspond to the expansion of atomic orbitals defined in the local coordinate frame of a given metal-ligand pair over orbitals defined with respect to a common coordination frame and are written via the Wigner D functions (see Fig. 6 in the Appendix B). Assuming in Eq. (24) the same $E(4p)$ orbital energy for three $4p_k$(Br) orbitals, we can define quantities

$$A_{ij} = \sum_{n=1,2,3} \sum_{k=0,\pm 1} \langle 4f_i|h|4p_k(L_n)\rangle\langle 4p_k(L_n)|h|3d_j\rangle, \qquad (25)$$

which, being divided by the common energy denominator $E(4p \rightarrow fd)$ (24), determine the contribution to t_{ij} from the $4p_k(L_n)$ orbitals of the bridging bromine atoms. Here $4p_k(L_n)$ is the $4p$ orbital of the nth bridging bromine atom with a definite projection of the orbital momentum k on the common C_3 axis.

For the C_{3v} point symmetry of the idealized structure of $YbCrBr_9^{3-}$ (Fig. 2), there are only six independent nonvanishing A_{ij} quantities (and, therefore, six independent t_{ij} transfer integrals) connecting $4f_i$ and $3d_j$ orbitals with $i = j$ and $i = j \pm 3$ only, which can be expressed via the $\sigma(fp)$, $\pi(fp)$, $\sigma(dp)$, and $\pi(dp)$ parameters (Table II).

Similarly, contributions from the $4s$(Br) orbitals can be expressed via two resonance integrals $\sigma(fs) = \langle 4f_0|h|4s\rangle$ and $\sigma(ds) = \langle 3d_0|h|4s\rangle$, corresponding to the σ overlap between metal orbitals and $4s$(Br) orbitals for a given Yb-Br or Cr-Br pair. Again, in Eq. (23) we can define quantities

$$B_{ij} = \sum_{n=1,2,3} \langle 4f_i|h|4s(L_n)\rangle\langle 4s(L_n)|h|3d_j\rangle, \qquad (26)$$

determining contributions from $4s$(Br) orbitals, $B_{ij}/E(4s \rightarrow fd) \rightarrow t_{ij}$. They are expressed via $\sigma(fs)$, and $\sigma(dp)$ resonance integrals in Table II. Details of the calculations of A_{ij} and B_{ij} are given in Appendix B.

TABLE II. The A_{ij} and B_{ij} quantities in the idealized model $YbCrBr_9^{3-}$ dimer. Details of calculations of A_{ij} and B_{ij} are given in the Appendix B.

A_{00}	$-\frac{8}{9}\pi(dp)\sigma(fp) + \frac{\sqrt{6}}{9}\pi(dp)\pi(fp)$
$A_{11} = A_{-1-1}$	$\frac{\sqrt{6}}{18}\sigma(dp)\sigma(fp) - \frac{\sqrt{2}}{9}\pi(dp)\sigma(fp) - \sigma(dp)\pi(fp)$
$A_{22} = A_{-2-2}$	$-\frac{\sqrt{15}}{18}\sigma(dp)\sigma(fp) - \frac{2\sqrt{5}}{9}\pi(dp)\sigma(fp) - \frac{\sqrt{30}}{6}\pi(dp)\pi(fp)$
$A_{30} = -A_{-30}$	$2\frac{\sqrt{10}}{9}\pi(dp)\sigma(fp) - \frac{\sqrt{15}}{18}\pi(dp)\pi(fp)$
$A_{2-1} = -A_{-21}$	$-\frac{\sqrt{30}}{18}\sigma(dp)\sigma(fp) + \frac{\sqrt{10}}{9}\pi(dp)\sigma(fp) + \frac{\sqrt{15}}{6}\pi(dp)\pi(fp)$
$A_{1-2} = -A_{-12}$	$-\frac{\sqrt{3}}{18}\sigma(dp)\sigma(fp) - \frac{2}{9}\pi(dp)\sigma(fp) + \frac{\sqrt{2}}{2}\sigma(dp)\pi(fp)$
B_0	0
$B_{11} = B_{-1-1}$	$\frac{1}{\sqrt{6}}\sigma(ds)\sigma(fs)$
$B_{22} = B_{-2-2}$	$\frac{\sqrt{15}}{6}\sigma(ds)\sigma(fs)$
$B_{30} = B_{-30}$	0
$B_{2-1} = -B_{-21}$	$\frac{\sqrt{30}}{6}\sigma(ds)\sigma(fs)$
$B_{1-2} = -B_{-12}$	$\frac{\sqrt{3}}{6}\sigma(ds)\sigma(fs)$

The $\sigma(fp)$, $\pi(fp)$, $\sigma(dp)$, $\pi(dp)$, $\sigma(fs)$, and $\sigma(dp)$ resonance integrals can be calculated using the approximate Wolfsberg-Helmholtz formula[44]

$$\sigma(fp)=\langle 4f_0|h|4p_0\rangle=K[E(4f)+E(4p)]S_\sigma(4f,4p), \tag{27a}$$

$$\pi(fp)=\langle 4f_{\pm 1}|h|4p_{\pm}\rangle=K[E(4f)+E(4p)]S_\pi(4f,4p), \tag{27b}$$

$$\sigma(dp)=\langle 3d_0|h|4p_0\rangle=K[E(3d)+E(4p)]S_\sigma(3d,4p), \tag{27c}$$

$$\pi(dp)=\langle 4f_{\pm 1}|h|4p_{\pm 1}\rangle=K[E(4f)+E(4p)]S_\pi(3d,4p), \tag{27d}$$

$$\sigma(fs)=\langle 4f_0|h|4s\rangle=K[E(4f)+E(4s)]S_\sigma(4f,4s), \tag{27e}$$

$$\sigma(ds)=\langle 3d_0|h|4s\rangle=K[E(3d)+E(4s)]S_\sigma(3d,4s), \tag{27f}$$

where K is a numerical coefficient (which is normally taken as $K=0.875$ or 1) and $S_\sigma(4f,4p)$, $S_\pi(4f,4p)$, $S_\sigma(3d,4p)$, $S_\pi(3d,4p)$, $S_\sigma(4f,4s)$, and $S_\sigma(3d,4s)$ are σ and π overlap integrals between the respective metal and ligand orbitals. In further calculations, a value $K=1$ is used. Although in the model $YbCrBr_9^{3-}$ dimer the $YbBr_6$ and $CrBr_6$ polyhedra are assumed to be regular octahedra with the equal Cr-Br and Yb-Br distances, in the calculations of overlap integrals we use the actual distances between the metal ions and bridging bromide ligands in the $Yb_2Br_9^{3-}$ and $Cr_2Br_9^{3-}$ dimers, 2.86 and 2.65 Å, respectively.[31,32] The overlap integrals were calculated with four-exponent radial functions for $4f$ orbitals[45] and double-zeta radial functions for $3d$(Cr) orbitals;[46] the radial functions for the $4s$(Br) and $4p$(Br) orbitals were taken from Ref. 47. We obtained $S_\sigma(4f,4p)=-0.0187$, $S_\pi(4f,4p)=0.0091$, $S_\sigma(3d,4p)=0.122$, $S_\pi(3d,4p)=-0.054$, $S_\sigma(4f,4s)=0.0102$, and $S_\sigma(3d,4s)=0.077$. The orbital energies $E(3d)=-11$, $E(4p)=-14$, and $E(4s)=-22$ eV were taken with a minor rounding-off from the standard parametrization used in Extended Huckel calculations,[46,47] and the typical orbital energy $E(4f)=-10$ eV was used for f electrons.[48–50] Using these data, the resonance integrals, A_{ij} and B_{ij} quantities, and the energy denominators (24) were calculated. Then the contributions from the $4s$(Br) and $4p$(Br) orbitals to the transfer integrals were determined and the $t(4f_i\text{-}3d_j)$ transfer integrals were calculated, which are given in Table III. In accordance with the C_{3v} symmetry of the $YbCrBr_9^{3-}$ dimer, there are eleven nonvanishing transfer integrals, which connect $4f_i$ and $3d_j$ orbitals with $i-j=0$ or ± 3; of these, only six t_{ij} are independent due to the relations $t_{30}=-t_{-30}$, $t_{2-1}=-t_{-21}$, $t_{1-2}=-t_{1-2}$, and $t_{ii}=t_{-i-i}$ (Table III).

IV. RESULTS AND DISCUSSION

In this section we analyze in detail the mechanism of the Yb^{3+}-Cr^{3+} superexchange interactions in the $YbCrBr_9^{3-}$ dimer and discuss the results of numerical calculations of the $4f\text{-}3d$ exchange spin Hamiltonian. In particular, we focus on the interplay between various contributions from numerous individual states of the $4f^{12}\text{-}3d^4$ and $4f^{14}\text{-}3d^2$ CT configurations to the parameters of the highly anisotropic $4f\text{-}3d$ exchange spin-Hamiltonian of the $YbCrBr_9^{3-}$ dimer and the symmetry relationships between the matrix elements.

A. The ground electronic states of the Yb and Cr centers in the $YbCrBr_9^{3-}$ dimer

The ground electronic state of the Yb^{3+} ion in the regular $YbBr_6^{3-}$ octahedron is the Γ_6 Kramers doublet resulting from the CF splitting of the lowest $^2F_{7/2}$ multiplet (Fig. 3). Since there are no Γ_6 states among CF levels of the excited $^2F_{5/2}$ multiplet, the Γ_6 ground state is of pure $^2F_{7/2}$ character. This implies that the wave functions of the Γ_6 ground doublet in the regular $YbBr_6^{3-}$ octahedron are determined by the symmetry only and are insensitive to the strength of the CF splitting. As a result, the exchange parameters in the $YbCrBr_9^{3-}$ dimer are also insensitive to this CF splitting.

With the quantization axis C_3 (Fig. 2), the wave functions of the Γ_6 doublet can be written in terms of the $|JM_J\rangle$ wave functions of the ground $^2F_{7/2}$ multiplet

$$|\Gamma_{6,}-\tfrac{1}{2}\rangle=\frac{1}{\sqrt{54}}[-\sqrt{35}|\tfrac{5}{2}\rangle-\sqrt{14}|-\tfrac{1}{2}\rangle+\sqrt{5}|-\tfrac{7}{2}\rangle], \tag{28a}$$

$$|\Gamma_{6,}+\tfrac{1}{2}\rangle=\frac{1}{\sqrt{54}}[-\sqrt{35}|-\tfrac{5}{2}\rangle+\sqrt{14}|\tfrac{1}{2}\rangle+\sqrt{5}|\tfrac{7}{2}\rangle]. \tag{28b}$$

They can also be expressed via the $4f_l$ orbitals ($l=-3,-2,...,3$) and the spin wave functions $\alpha(+\frac{1}{2})$ and $\beta(-\frac{1}{2})$

$$|\Gamma_{6,}-\tfrac{1}{2}\rangle=\frac{1}{\sqrt{54}}\{-\sqrt{5}[f_{-3}\alpha]+\sqrt{30}[f_{-2}\beta]+\sqrt{8}[f_0\alpha]-\sqrt{6}[f_1\beta]+\sqrt{5}[f_3\alpha]\}, \tag{29a}$$

$$|\Gamma_{6,}+\tfrac{1}{2}\rangle=\frac{1}{\sqrt{54}}\{-\sqrt{5}[f_3\beta]+\sqrt{30}[f_2\alpha]-\sqrt{8}[f_0\beta]+\sqrt{6}[f_{-1}\alpha]+\sqrt{5}[f_{-3}\beta]\}, \tag{29b}$$

where $[f_l\sigma]$ denotes the orbital and spin quantum numbers of a hole in the $4f^{13}$ configuration; in the electron representation, $[f_l\sigma]$ is a Slater determinant with all $4f$ orbitals doubly occupied except for the $4f_l$ orbital with the spin projection $\sigma=\alpha$ or β. The signs of the effective spin projection of the $|\Gamma_{6,}-\frac{1}{2}\rangle$ and $|\Gamma_{6,}+\frac{1}{2}\rangle$ components of the Γ_6 doublet are chosen to match the transformational properties of the $S=\frac{1}{2}$ wave functions α and β with respect to rotations around the C_3 axis by angles $\varphi=\pm 2\pi/3$: $|\Gamma_{6,}-\frac{1}{2}\rangle\rightarrow e^{-i\varphi/2}|\Gamma_{6,}-\frac{1}{2}\rangle$ and $\Gamma_{6,}+\frac{1}{2}\rangle\rightarrow e^{i\varphi/2}|\Gamma_{6,}+\frac{1}{2}\rangle$. This brings into accordance the transformation properties of wave functions of the effective spin $S_{Yb}=\frac{1}{2}$ and those of the true spin $S_{Cr}=\frac{3}{2}$. Note that the sign of the projection of the magnetic momentum of the Yb^{3+} ion is opposite to the sign of the spin projection $\mu_z(-\frac{1}{2})=+4/3\mu_B$, $\mu_z(+\frac{1}{2})=-4/3\mu_B$. This implies that

TABLE III. $t(4f_i-3d_j)$ transfer integrals in the $YbCrBr_9^{3-}$ dimer.

$t(4f_i-3d_j)$ transfer integrals, cm^{-1}					
Contributions from the $4p$(Br) states					
	$3d_{-2}$	$3d_{-1}$	$3d_0$	$3d_1$	$3d_2$
$4f_{-3}$	0	0	−1154	0	0
$4f_{-2}$	620	0	0	−1038	0
$4f_{-1}$	0	−2236	0	0	−1105
$4f_0$	0	0	−1459	0	0
$4f_1$	1105	0	0	−2236	0
$4f_2$	0	1038	0	0	620
$4f_3$	0	0	1154	0	0
Contributions from the $4s$(Br) states					
	$3d_{-2}$	$3d_{-1}$	$3d_0$	$3d_1$	$3d_2$
$4f_{-3}$	0	0	0	0	0
$4f_{-2}$	377	0	0	−534	0
$4f_{-1}$	0	239	0	0	−169
$4f_0$	0	0	0	0	0
$4f_1$	169	0	0	239	0
$4f_2$	0	534	0	0	377
$4f_3$	0	0	0	0	0
Total					
	$3d_{-2}$	$3d_{-1}$	$3d_0$	$3d_1$	$3d_2$
$4f_{-3}$	0	0	−1154	0	0
$4f_{-2}$	997	0	0	−1572	0
$4f_{-1}$	0	−1997	0	0	−1274
$4f_0$	0	0	−1459	0	0
$4f_1$	1274	0	0	−1997	0
$4f_2$	0	1572	0	0	997
$4f_3$	0	0	1154	0	0

in the regular $YbBr_6^{3-}$ octahedron assumed here, the g tensor of the ground Γ_6 doublet is negative and isotropic ($g_x=g_y=g_z=-\frac{8}{3}$). Since in the parent $Yb_2Br_9^{3-}$ dimer $YbBr_6$ octahedra are somewhat distorted, the g tensor of Yb^{3+} is expected to be anisotropic. Note that the phases of the wave functions $|\Gamma_{6,}-\frac{1}{2}\rangle$ and $|\Gamma_{6,}+\frac{1}{2}\rangle$ in Eqs. (28) and (29) are consistent with the time-reversal symmetry $|\Gamma_{6,}+\frac{1}{2}\rangle\rightarrow|\Gamma_{6,}-\frac{1}{2}\rangle$ and $|\Gamma_{6,}-\frac{1}{2}\rangle\rightarrow-|\Gamma_{6,}+\frac{1}{2}\rangle$. As can be seen from Eq. (29), $4f$ states with different l and σ are strongly mixed to each other thus implying that the spin of Yb^{3+} is not a good quantum number. It is important, that the Γ_6 ground state is separated from the first excited state by an energy gap being much larger [114 cm^{-1} in the $Cs_3Yb_2Br_9$ (Ref. 42)] than the Yb^{3+}-Cr^{3+} exchange parameters [about 5 cm^{-1} (Ref. 26)], so that these states cannot admix.

The wave function of the ${}^4A_{2g}$ ground state of the octahedrally coordinated Cr^{3+} ion in the widely used tetragonal quantization is represented by a single Slater determinant $\mathrm{Det}(d_{xy}\alpha,d_{zx}\alpha,d_{yz}\alpha)$ incorporating three t_{2g} electrons with parallel spins (for the maximum spin projection $M_s=\frac{3}{2}$.) For the trigonal quantization, the ${}^4A_{2g}$ state is represented by a sum of several determinants

$$\frac{\sqrt{2}}{3}\{\mathrm{Det}(d_2\alpha,d_1\alpha,d_0\alpha)-\mathrm{Det}(d_0\alpha,d_{-1}\alpha,d_{-2}\alpha)\}+\frac{2}{3}\mathrm{Det}(d_2\alpha,d_0\alpha,d_{-2}\alpha)+\frac{1}{3}\mathrm{Det}(d_1\alpha,d_0\alpha,d_{-1}\alpha), \tag{30}$$

where $3d$ orbitals are given in the orbital momentum representation. It is important to note that the wave function of the ${}^4A_{2g}$ ground state of Cr^{3+} is insensitive even to rather strong distortions of the octahedral ligand environment. This means that deviations from the strict octahedral symmetry of the chromium center in the real $YbCrBr_9^{3-}$ dimer would not influence much the orbital composition of the wave function (30). Again, since the ground state of the Cr^{3+} ion in the $CrBr_6$ octahedron is well isolated from the excited states (by about 14 000 cm^{-1}), exchange interactions represent therefore only a small perturbation to the CF splitting energy and thus the mixing with other CF states can be neglected.

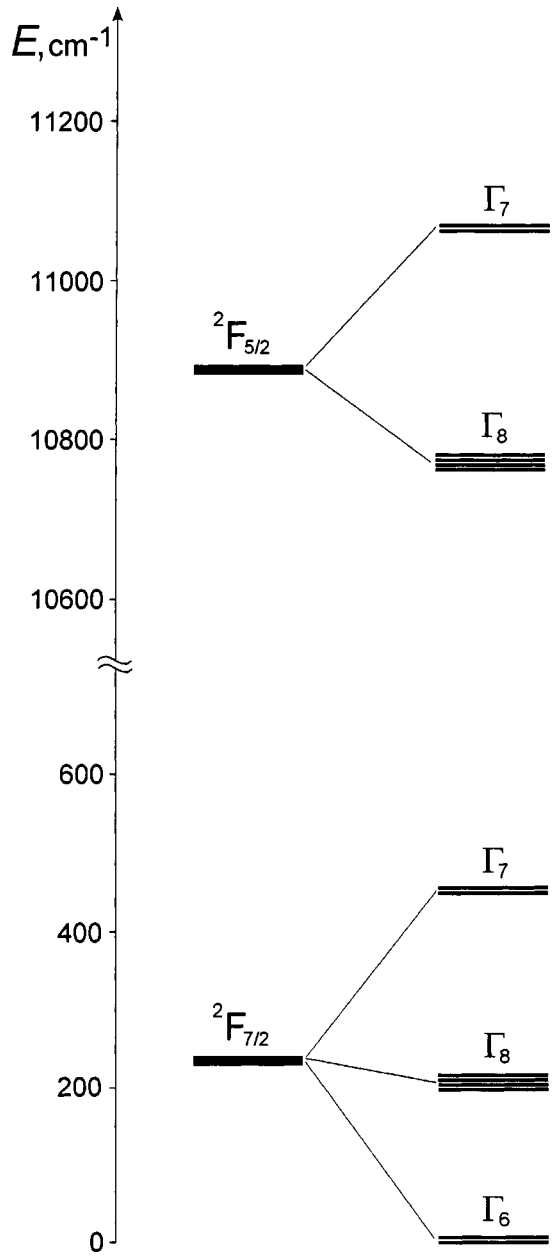

FIG. 3. The structure of crystal-field energy levels of Yb^{3+} ion in the octahedral ligand surrounding.

B. Matrix elements of the effective exchange Hamiltonian

With the use of the parameters determined in the previous section, the full set of $\langle m,M_s|H_{\rm eff}|m',M_s'\rangle$ matrix elements of the effective exchange Hamiltonian was numerically calculated using the program outlined above. In these calculations, all CT states resulting from the $4f\rightarrow 3d$ and $4f\leftarrow 3d$ electron transfers were taken into account, which involve 19 110 and 45 individual CT states for the $4f^{12}$-$3d^4$ and $4f^{14}$-$3d^2$ CT configurations, respectively. These are drawn in Fig. 4 in the actual energy scale. We can see that even for a rather simple $4f^{13}$-$3d^3$ pair the energy structure of the CT band is very complicated. The spectrum of the $4f^{12}$ configuration involves 91 states with the total energy extension of about 9 eV. The energy spectrum of the $3d^4$ configuration of the chromium center involves 210 states and spans over the range of 11 eV. The total energy width of the $4f\rightarrow 3d$ CT band of the $YbCrBr_9^{3-}$ dimer is therefore about 20 eV, which is considerably larger than the typical CT energy (5–10 eV). The electronic structure of the $4f\leftarrow 3d$ CT band is less complicated, since the ytterbium center has a closed $4f^{14}$ configuration. However, even in this case the total width of the CT band (which is equal to that of the $3d^2$ configuration) is comparable with the $U_0(A\leftarrow B)$ CT gap (Fig. 4). In these calculations, the CF splittings of multiplets of the $4f^{12}$ CT configuration of ytterbium are not taken into account since they are negligibly small as compared to the CT energies.

Calculations performed at various $U_0(A\rightarrow B)$ and $U_0(A\leftarrow B)$ CT energies show that there are highly symmetric relations between the matrix elements. This is exemplified by Table IV, which presents the matrix elements $\langle m,M_s|H_{\rm eff}|m',M_s'\rangle$ and the separate contributions from the $4f^{12}$-$3d^4$ and $4f^{14}$-$3d^2$ CT states calculated at $U_0(A\rightarrow B)=10$ eV and $U_0(A\leftarrow B)=5$ eV. Most of these matrix elements are zero except for diagonal ones with $m=m'$ and $M_s=M_s'$ and the only nondiagonal matrix elements with $|m-m'|=1$ and $m+M_s=m'+M_s'$. In addition, the diagonal matrix elements have the form

$$\langle m,M_s|H_{\rm eff}|m,M_s\rangle = X + YmM_s, \tag{31}$$

while the nondiagonal matrix elements obey the relations

$$\langle m,M_s|H_{\rm eff}|m-1,M_s+1\rangle = Z\sqrt{3/4-m(m-1)} \times\sqrt{S(S+1)-M_s(M_s+1)}, \tag{32a}$$

$$\langle m,M_s|H_{\rm eff}|m+1,M_s-1\rangle = Z\sqrt{3/4-m(m+1)} \times\sqrt{S(S+1)-M_s(M_s-1)}, \tag{32b}$$

where *X, Y, Z* are some constants, which do not depend on m or M_s, (but different for $4f\rightarrow 3d$ and $4f\leftarrow 3d$ electron transfer contributions). The microscopic origin of these regularities is discussed below.

From these results we can determine the spin Hamiltonian $H_{4f\text{-}3d}$ of the Yb^{3+}-Cr^{3+} exchange interaction in the $YbCrBr_9^{3-}$ dimer. Indeed, matrix elements of the spin Hamiltonian

$$H_{4f\text{-}3d} = A_0 + J_z S_{\rm Yb}^z S_{\rm Cr}^z + J_\perp (S_{\rm Yb}^x S_{\rm Cr}^x + S_{\rm Yb}^y S_{\rm Cr}^y), \tag{33}$$

coincide with the matrix elements of the effective exchange Hamiltonian calculated above provided that $A_0=X$, $J_z=Y$, and $J_\perp=2Z$. For a Yb^{3+}-Cr^{3+} pair, these exchange parameters can be directly expressed via the $\langle m,M_s|H_{\rm eff}|m',M_s'\rangle$ matrix elements

$$J_z = \frac{2}{3}\left[\left\langle +\tfrac{1}{2},\tfrac{3}{2}\middle|H_{\rm eff}\middle|+\tfrac{1}{2},\tfrac{3}{2}\right\rangle - \left\langle -\tfrac{1}{2},\tfrac{3}{2}\middle|H_{\rm eff}\middle|-\tfrac{1}{2},\tfrac{3}{2}\right\rangle\right]. \tag{34a}$$

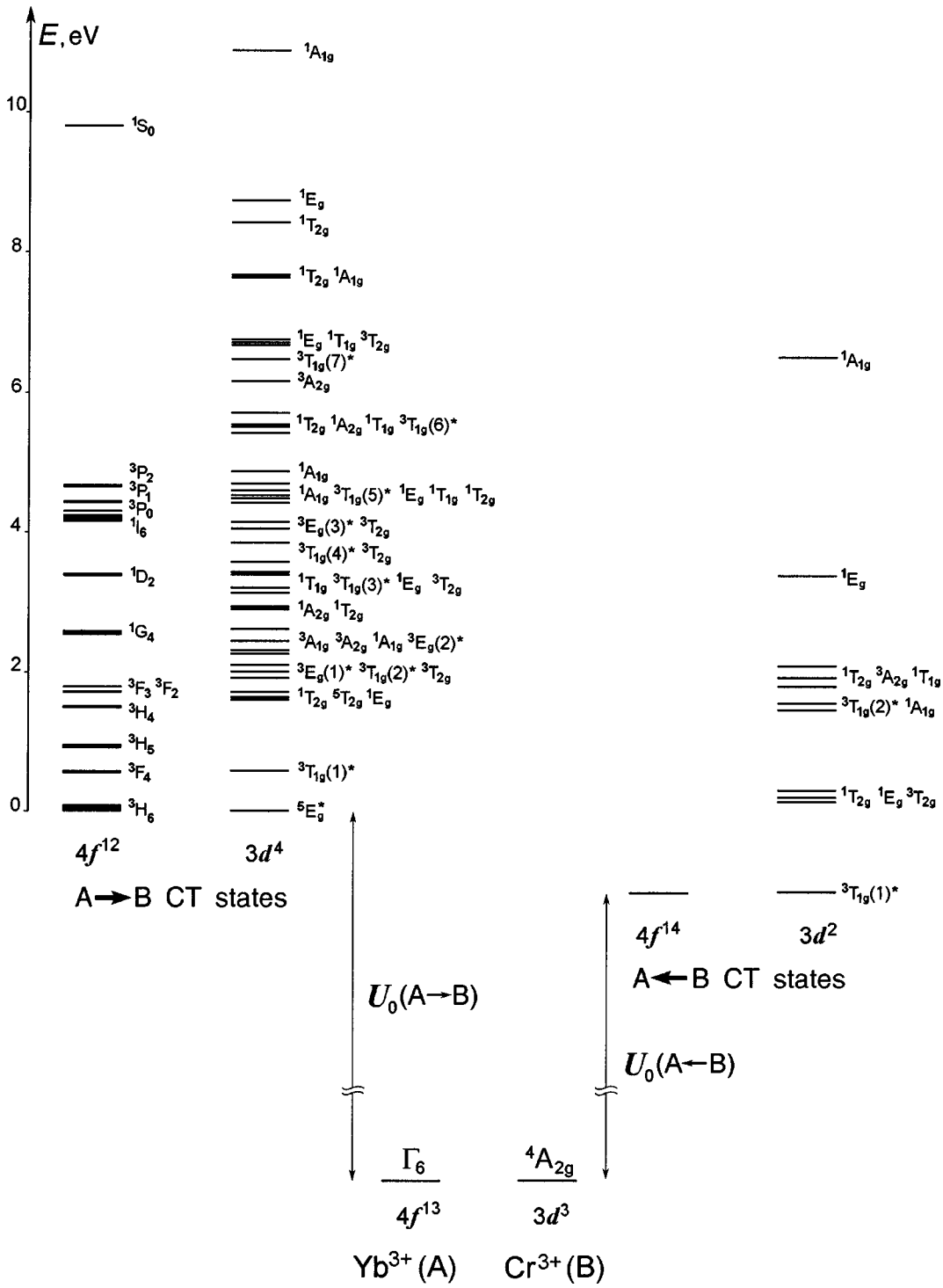

FIG. 4. The energy structure of the $4f^{12}$-$3d^4$ and $4f^{14}$-$3d^2$ CT configurations of the $YbCrBr_9^{3-}$ dimer. The energies of CT states are given in the real energy scale. The contributive ^5E_g, ^3E_g, and $^3T_{1g}$ levels of the $3d^4$ and $3d^2$ configurations of chromium are enumerated and marked by star.

$$J_\perp = \langle -\tfrac{1}{2}, \tfrac{1}{2} | H_{\text{eff}} | +\tfrac{1}{2}, -\tfrac{1}{2} \rangle, \tag{34b}$$

$$A_0 = \tfrac{1}{2}[\langle +\tfrac{1}{2}, \tfrac{3}{2} | H_{\text{eff}} | +\tfrac{1}{2}, \tfrac{3}{2} \rangle + \langle -\tfrac{1}{2}, \tfrac{3}{2} | H_{\text{eff}} | -\tfrac{1}{2}, \tfrac{3}{2} \rangle]. \tag{34c}$$

Note that, according to the usual convention, the positive sign of exchange parameters corresponds to a ferromagnetic spin coupling, and the negative sign to an antiferromagnetic coupling. In this convention, the sign at the exchange parameter in the spin Hamiltonian is therefore chosen to be negative, such as $-J\mathbf{S}_A \cdot \mathbf{S}_B$ in the case for the isotropic Heisenberg Hamiltonian. However, in our case one should remember that the g tensor of the Γ_6 Kramers doublet is negative ($g = -\frac{8}{3}$), i.e., the effective spin $\mathbf{S}$ of the Yb^{3+} ion

TABLE IV. $\langle m,M_s|H_{\rm eff}|m',M_s'\rangle$ matrix elements (other $\langle m,M_s|H_{\rm eff}|m',M_s'\rangle$ matrix elements are zero) and exchange parameters of the effective exchange Hamiltonian $H_{4f\text{-}3d}=A_0+J_z S^z_{\rm Yb}S^z_{\rm Cr}+J_\perp(S^x_{\rm Yb}S^x_{\rm Cr}+S^y_{\rm Yb}S^y_{\rm Cr})$ in the $YbCrBr_9^{3-}$ dimmer calculated at $U_0(A\rightarrow B)=10$ eV and $U_0(A\leftarrow B)=5$ eV. Contributions from the $4f^{12}$-$3d^4$ and $4f^{14}$-$3d^2$ CT states are indicated separately.

Diagonal $\langle m,M_s\|H_{\rm eff}\|m',M_s'\rangle$ matrix elements ($m=m',M_s=M_s'$), cm^{-1}						
m	M_s	m'	M_s'	$4f^{12}$-$3d^4$	$4f^{14}$-$3d^2$	Total
−1/2	−3/2	−1/2	−3/2	−258.8772	−7.4549	−266.3321
−1/2	−1/2	−1/2	−1/2	−258.7276	−5.1306	−263.8582
−1/2	1/2	−1/2	1/2	−258.5781	−2.8063	−261.3844
−1/2	3/2	−1/2	3/2	−258.4285	−0.4820	−258.9105
+1/2	−3/2	+1/2	−3/2	−258.4285	−0.4820	−258.9105
+1/2	−1/2	+1/2	−1/2	−258.5781	−2.8063	−261.3844
+1/2	1/2	+1/2	1/2	−258.7276	−5.1306	−263.8582
+1/2	3/2	+1/2	3/2	−258.8772	−7.4549	−266.3321
Nondiagonal $\langle m,M_s\|H_{\rm eff}\|m',M_s'\rangle$ matrix elements, cm^{-1}						
−1/2	3/2	+1/2	1/2	+3.7936	−0.2783	+3.5153
−1/2	1/2	+1/2	−1/2	+4.3805	−0.3214	+4.0591
−1/2	−1/2	+1/2	−3/2	+3.7936	−0.2783	+3.5153
+1/2	−3/2	−1/2	−1/2	+3.7936	−0.2783	+3.5153
+1/2	−1/2	−1/2	1/2	+4.3805	−0.3214	+4.0591
+1/2	1/2	−1/2	3/2	+3.7936	−0.2783	+3.5153
Exchange parameters, cm^{-1} [a]				$A_0=-258.6528$ $J_z=-0.2991$ $J_\perp=+4.3805$	$A_0=-3.9685$ $J_z=-4.6486$ $J_\perp=-0.3214$	$A_0=-262.6203$ $J_z=-4.9477$ $J_\perp=+4.0591$

[a]The sign of J_z and $J_\perp$ corresponds to the true sign of the exchange parameters $J_z<0$ (antiferromagnetic) and $J_\perp>0$ (ferromagnetic), see the text for details.

is antiparallel to its magnetic momentum μ. Therefore, since actual ferromagnetic and antiferromagnetic interactions refer to the parallel and antiparallel orientations of the magnetic moments on Yb^{3+} and Cr^{3+} ions, the formal sign of the exchange parameters J_z and $J_\perp$ corresponding to the orientation of the effective spin of Yb^{3+} and the true spin of Cr^{3+} should be reversed. Alternatively, the negative sign at the exchange parameters (J_z and $J_\perp$) in the spin Hamiltonian should be changed to the positive sign; we have done so in the spin Hamiltonian (33) in order to follow the usual sing convention. Thus, the positive exchange parameter corresponds now to the antiparallel orientation of the spins of Yb^{3+} and Cr^{3+} and to the parallel orientation of their magnetic moments (and vice versa for the negative exchange parameter).

Note that, in accordance with the C_{3v} symmetry of the $YbCrBr_9^{3-}$ model dimer, the spin Hamiltonian $H_{\rm eff}$ (33) has the axial symmetry. In particular, the Dzyaloshinskii-Moriya antisymmetric term $\mathbf{A}[\mathbf{S}_{\rm Yb}\times\mathbf{S}_{\rm Cr}]$ is vanishing in the spin Hamiltonian (33), being consistent with the symmetry condition $\mathbf{A}=0$ for the C_{3v} group.[20] The parameter A_0 includes spin-independent contributions to the total energy of the system from $4f\rightarrow 3d$ and $4f\leftarrow 3d$ electron transfers, while J_z and $J_\perp$ describe spin-dependent contributions. Using Eq. (34) and the sets of the $\langle m,M_s|H_{\rm eff}|m',M_s'\rangle$ matrix elements obtained at various CT energies $U_0(A\rightarrow B)$ and $U_0(A\leftarrow B)$, we calculated the A_0, J_z, and $J_\perp$ exchange parameters and the separate contributions from the $A\rightarrow B$ and $A\leftarrow B$ CT states. The dependence of the contributions to J_z and $J_\perp$ from the $4f^{12}$-$3d^4$ and $4f^{14}$-$3d^2$ configurations on the CT energies is shown in Fig. 5. The contributions to J_z and $J_\perp$ from the $4f^{12}$-$3d^4$ configuration are not proportional to $U_0(A\rightarrow B)^{-1}$, especially for the J_z parameters, which changes the sign from ferro- to antiferromagnetic around 8 eV [Fig. 5(a)]

These contributions show quite different behavior: the contribution from the $4f^{12}$-$3d^4$ configuration corresponds to an almost purely ferromagnetic XY spin Hamiltonian [$J_\perp>0$ and $J_\perp\gg|J_z|$, Fig. 5(a)], while the contribution from the $4f^{14}$-$3d^2$ configuration gives rise to an almost pure antiferromagnetic Ising-like interaction [$J_z<0$ and $|J_z|\gg|J_\perp|$, Fig. 5(b)]. In particular, at the CT energies $U_0(A\rightarrow B)=10$ eV and $U_0(A\leftarrow B)=5$ eV estimated above for a Yb^{3+}-Cr^{3+} pair, the exchange parameters are $A_0=-262.62$, $J_z=-4.95$, and $J_\perp=+4.06\ cm^{-1}$ (with the separate contributions $A_0=-258.65$, $J_z=-0.30$, $J_\perp=+4.38\ cm^{-1}$ from the $4f^{12}$-$3d^4$ configuration and $A_0=-3.97$, $J_z=-4.65$, $J_\perp=-0.32\ cm^{-1}$ from the $4f^{14}$-$3d^2$ configuration, Table IV). These are well consistent with the experimental exchange parameters of $YbCrBr_9^{3-}$, $J_z=-5.16$ and $J_\perp=+4.19\ cm^{-1}$, obtained from inelastic neutron scattering experiments.[26] Quantitatively, this coincidence should not be overemphasized, since a very idealized structural model was assumed for the $YbCrBr_9^{3-}$ dimer and a number of approximations were used in the spin-Hamiltonian calculations.

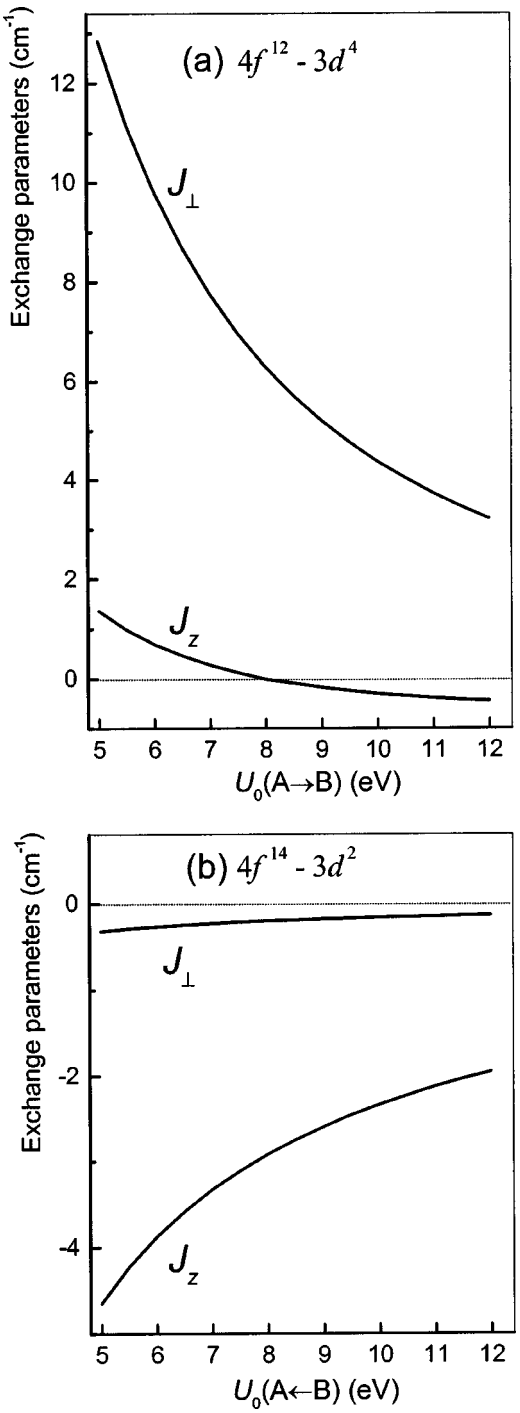

FIG. 5. The variation of the contributions to the J_z and $J_\perp$ exchange parameters from the $4f^{12}$-$3d^4$ and $4f^{14}$-$3d^2$ configurations with increasing the $U_0(A\rightarrow B)$ and $U_0(A\leftarrow B)$ CT energies.

However, these results clearly indicate that the kinetic exchange mechanism is adequate to the description of the spin coupling between lanthanide and transition metal ions in insulators and the model developed above can provide a consistent quantitative analysis of the $4f$-$3d$ superexchange interactions in really existing lanthanide compounds. Below we analyze this mechanism in more detail.

C. Contributions to the exchange parameters from individual CT states

In this section we will show that the regularities observed from numerical calculations are not accidental and, moreover, not specific to the matrix elements of the effective exchange Hamiltonian for the $YbCrBr_9^{3-}$ dimer. In particular, the same regularities show up Ln^{3+}-M^{n+} ($Ln^{3+}=Ce^{3+}$, Yb^{3+}; $M^{n+}=Cr^{3+}$, Mn^{2+}, and Ni^{2+}) corner-sharing bioctahedral dimers of the C_{4v} symmetry.[35] Actually, the relations (31) and (32) originate from general dependence of the $\langle m,M_s|H_{AB}|\Xi_{pq}(A\rightarrow B;S'M')\rangle$ matrix elements on the spin projection M_s at the $3d$ ion and from selection rules for matrix elements related to the symmetry of the $4f$-$3d$ dimer. Here we outline the underlying reason for their origin.

Since the $\Phi_0(3d^M;SM_s)$ ground state of the basic configurations of the transition metal center B ($^4A_{2g}$ state in the case of the Cr^{3+} ion) is connected to the $\Phi_q(3d^{M+1};S'M')$ CT states via the $4f\rightarrow 3d$ transfer of one electron, non-zero matrix elements $\langle m,M_s|H_{AB}|\Xi_{pq}(A\rightarrow B;S'M')\rangle$ can only appear if $S'=S\pm\frac{1}{2}$ and $M'=M_s\pm\frac{1}{2}$. One more selection rule is related to the transformational properties of the wave functions $|m,M_s\rangle$ and $\Xi_{pq}(A\rightarrow B;S'M')$ with respect to rotations by the angles $\varphi=\pm 2\pi/3$ around the C_3 axis of the $YbCrBr_9^{3-}$ dimer. Consider the transformation properties of the spin and orbital components of these wave functions. As noted above, the $|\Gamma_{6,}-\frac{1}{2}\rangle$ and $|\Gamma_{6,}+\frac{1}{2}\rangle$ wave functions of Yb^{3+} transform similar to the components of the true spin $S=\frac{1}{2}$, $|\Gamma_{6,}-\frac{1}{2}\rangle\rightarrow e^{-i\varphi/2}|\Gamma_{6,}-\frac{1}{2}\rangle$ and $|\Gamma_{6,}+\frac{1}{2}\rangle\rightarrow e^{i\varphi/2}|\Gamma_{6,}+\frac{1}{2}\rangle$. The orbitally nondegenerate wave function $\Phi_0(3d^M;SM_s)\rangle$ of Cr^{3+} transforms similar to the $|SM_s\rangle$ spin wave function, $\Phi_0(3d^M;SM_s)\rangle\rightarrow e^{iM_s\varphi}\Phi_0(3d^M;SM_s)\rangle$. Therefore, $|m,M_s\rangle$ is multiplied by $e^{i(m+M_s)\varphi}$ upon the rotation. In the C_{3v} group, the orbital part of the $\Xi_{pq}(A\rightarrow B;S'M')$ CT wave function can transform either as the angular momentum $L=0$ [if $\Xi_{pq}(A\rightarrow B;S'M')$ belongs to the A_1 or A_2 irreducible representation] or $L=1$ with the projections $M_L=\pm 1$ (for the E representation); below these cases are denoted as $\Xi_{pq}(A\rightarrow B;S'M')\in M_L=0$ and ± 1, respectively. Since the spin part of $\Xi_{pq}(A\rightarrow B;S'M')$ transforms as $\Xi_{pq}(A\rightarrow B;S'M')\rightarrow e^{iM'\varphi}\Xi_{pq}(A\rightarrow B;S'M')$, the $\Xi_{pq}(A\rightarrow B;S'M')$ wave functions multiplies by $e^{i(L_M+M')\varphi}$ upon the rotation. For the matrix element $\langle m,M_s|H_{AB}|\Xi_{pq}(A\rightarrow B;S'M')\rangle$ to be invariant, the phase factors of its two wave functions should coincide, i.e., $m+M_s=M_L+M'$. Therefore, the selection rules for non-zero matrix elements are determined by the set of conditions

$$S'=S\pm\tfrac{1}{2}, \tag{35a}$$

$$M'=M_s\pm\tfrac{1}{2}, \tag{35b}$$

$$m+M_s=M_L+M', \tag{35c}$$

according to which different cases are possible. Consider first the case of $S'=S-\frac{1}{2}$.

At fixed orbital indexes p and q of the $\Xi_{pq}(A\rightarrow B;S'M')$ CT states, there are four situations, in which the dependence of nonzero matrix elements on M_s is given by

$$\text{(a)}\quad S'=S-\tfrac{1}{2},M'=M_s+\tfrac{1}{2},\ \text{and}\ \Xi_{pq}(A\rightarrow B;S'M')\in M_L=0;$$
$$\langle+\tfrac{1}{2},M_s|H_{AB}|\Xi_{pq}(A\rightarrow B;S'M')\rangle=A(p,q)\sqrt{S-M_s}, \tag{36}$$

$$\text{(b)}\quad S'=S-\tfrac{1}{2},M'=M_s-\tfrac{1}{2},\ \text{and}\ \Xi_{pq}(A\rightarrow B;S'M')\in M_L=0;$$
$$\langle-\tfrac{1}{2},M_s|H_{AB}|\Xi_{pq}(A\rightarrow B;S'M')\rangle=B(p,q)\sqrt{S+M_s}, \tag{37}$$

$$\text{(c)}\quad S'=S-\tfrac{1}{2},M'=M_s+\tfrac{1}{2},\ \text{and}\ \Xi_{pq}(A\rightarrow B;S'M')\in M_L=+1;$$
$$\langle-\tfrac{1}{2},M_s|H_{AB}|\Xi_{pq}(A\rightarrow B;S'M')\rangle=C(p,q)\sqrt{S-M_s}, \tag{38}$$

$$\text{(d)}\quad S'=S-\tfrac{1}{2},M'=M_s-\tfrac{1}{2},\ \text{and}\ \Xi_{pq}(A\rightarrow B;S'M')\in M_L=-1;$$
$$\langle+\tfrac{1}{2},M_s|M_{AB}|\Xi_{pq}(A\rightarrow B;S'M')\rangle=D(p,q)\sqrt{S+M_s}. \tag{39}$$

Note that the factors $A(p,q)$, $B(p,q)$, $C(p,q)$, and $D(p,q)$ are independent on M_s or M'. These regularities can be obtained from direct calculations of the $\langle m,M_s|H_{AB}|\Xi_{pq}(A\rightarrow B;S'M')\rangle$ matrix elements taking into account the usual relationships between the spin wave functions $\Phi_0(3d^M;SM_s)$ and $\Phi_q(3d^{M+1};S'M')$ of the $3d$ center with different spin projections M_s and M'. In addition, the factors $A(p,q)$, $B(p,q)$, $C(p,q)$ and $D(p,q)$ are related to each other by the time-reversal symmetry

$$\langle+\tfrac{1}{2},M_s|H_{AB}|\Xi_{pq}(A\rightarrow B;S'M')\rangle=\pm\langle-\tfrac{1}{2},-M_s|H_{AB}|\Xi^T_{pq}(A\rightarrow B;S'-M')\rangle, \tag{40}$$

where $\Xi^T_{pq}(A\rightarrow B;S'-M')$ is a wave function resulted from the action of the time-reversal operator $\mathbf{T}$, $\Xi^T_{pq}(A\rightarrow B;S'-M')=\mathbf{T}\Xi_{pq}(A\rightarrow B;S'M')$; the plus or minus sign in Eq. (40) is chosen according to the orbital part of the wave function $\Xi_{pq}(A\rightarrow B;S'M')$. Due to the time-reversal symmetry, the $\Xi^T_{pq}(A\rightarrow B;S'-M')$ wave function is an eigenvector of the Hamiltonian of the dimer, that corresponds to a CT state with the same energy $E_{pq}(A\rightarrow B)$ as that of the original $\Xi_{pq}(A\rightarrow B;S'M')$ state. In the case, when $\Xi_{pq}(A\rightarrow B;S'M')\in M_L=0$, the wave function $\Xi^T_{pq}(A\rightarrow B;S'-M')$ coincides with $\Xi_{pq}(A\rightarrow B;S'-M')$ within the phase factor and thus describes the same CT state. Then we have

$$B(p,q)=\pm A(p,q). \tag{41}$$

The situation is different, when $\Xi_{pq}(A\rightarrow B;S'M')\in M_L=\pm 1$ (i.e., when the orbital part belongs to the E representation); again, the $\Xi^T_{pq}(A\rightarrow B;S'-M')$ wave function corresponds to a CT state with the same energy but has the opposite sign of the projection of the quasimomentum M_L. Therefore, the wave function $\Xi_{p'q'}(A\rightarrow B;S'M')=\Xi^T_{pq}(A\rightarrow B;S'M')$ (whose orbital indexes are denoted by p' and q') and the original wave function $\Xi_{pq}(A\rightarrow B;S'M')$ describes two individual states of the same doubly degenerate CT level of the E representation. Thus we obtain

$$C(p,q)=\pm D(p',q'). \tag{42}$$

From Eqs. (36)–(42) we can determine the contributions to the A_0, J_z, and $J_\perp$ exchange parameters from individual CT states. For instance, according to Eq. (36), in the case (a) the contribution from the $\Xi_{pq}(A\rightarrow B;S'M')$ CT state to the $\langle+\frac{1}{2},M_s|H_{\text{eff}}|+1/2,M_s\rangle$ diagonal matrix element is given by

$$-\frac{A(p,q)^2}{E_{pq}(A\rightarrow B)}(S-M_s). \tag{43}$$

According to Eqs. (37) and (41), the same CT state contributes also to the $\langle-\frac{1}{2},M_s|H_{\text{eff}}|-\frac{1}{2},M_s\rangle$ diagonal matrix elements

$$-\frac{A(p,q)^2}{E_{pq}(A\rightarrow B)}(S+M_s). \tag{44}$$

Therefore, the contribution from the $\Xi_{pq}(A\rightarrow B;S'M')$ CT state with $M_L=0$ (A_1 or A_2 representation of the C_{3v} group) to the $\langle m,M_s|H_{\text{eff}}|m,M_s\rangle$ diagonal matrix elements can be written as

$$x(p,q)+y(p,q)mM_s, \tag{45}$$

where $x(p,q)$ and $y(p,q)$ are given by

$$x(p,q)=-\frac{A(p,q)^2}{E_{pq}(A\rightarrow B)}S, \tag{46a}$$

$$y(p,q)=+\frac{2A(p,q)^2}{E_{pq}(A\rightarrow B)}, \tag{46b}$$

where $E_{pq}(A\rightarrow B)$ is the energy of the CT state. The term $x(p,q)$ corresponds to the contribution to the spin-independent part A_0; it is always negative. The term $y(p,q)mM_s$ corresponds to the $J_zS^z_{\text{Yb}}S^z_{\text{Cr}}$ operator in the $H_{4f\text{-}3d}$ spin Hamiltonian of the $4f$-$3d$ pair [Eq. (33)] and thus $y(p,q)$ represents the contribution to the J_z exchange parameter; note that for the $\Xi_{pq}(A\rightarrow B;S'M')$ CT states with $M_L=0$; it is always positive (i.e., antiferromagnetic with respect to the spin orientation, and ferromagnetic with respect to the magnetic momentum orientation, see above). It is important that these CT states contribute to the nondiagonal matrix elements $\langle+\frac{1}{2},M_s|H_{\text{eff}}|-\frac{1}{2},M_s+1\rangle$ and $\langle-\frac{1}{2},M_s|H_{\text{eff}}|+\frac{1}{2},M_s-1\rangle$ as well. Taking into account Eqs. (36), (37), and (41), we have

$$\pm\frac{A(p,q)^2}{E_{pq}(A\rightarrow B)}\sqrt{(S-M_s)(S+M_s+1)}\Rightarrow\langle+\tfrac{1}{2},M_s|H_{\text{eff}}|-\tfrac{1}{2},M_s+1\rangle, \tag{47a}$$

$$\pm\frac{A(p,q)^2}{E_{pq}(A\rightarrow B)}\sqrt{(S+M_s)(S-M_s+1)}\Rightarrow\langle-\tfrac{1}{2},M_s|H_{\text{eff}}|+\tfrac{1}{2},M_s-1\rangle. \tag{47b}$$

These contributions can be rewritten as

$$z(p,q)\sqrt{[3/4-m(m-1)][S(S+1)-M_s(M_s+1)]}\Rightarrow\langle m,M_s|M_{\text{eff}}|m-1,M_s+1\rangle, \tag{48a}$$

$$z(p,q)\sqrt{[3/4-m(m+1)][S(S+1)-M_s(M_s-1)]}\Rightarrow\langle m,M_s|H_{\text{eff}}|m+1,M_s-1\rangle, \tag{48b}$$

where

$$z(p,q)=\pm\frac{A(p,q)^2}{E_{pq}(A\rightarrow B)}. \tag{49}$$

As pointed out above, Eqs. (32) and (33), these nondiagonal matrix elements just correspond to the spin operator

$$\frac{J_\perp}{2}(S^+_{\text{Yb}}S^-_{\text{Cr}}+S^-_{\text{Yb}}S^+_{\text{Cr}})=J_\perp(S^x_{\text{Yb}}S^x_{\text{Cr}}+S^y_{\text{Yb}}S^y_{\text{Cr}}). \tag{50}$$

Therefore, the quantity $2z(p,q)$ represents the contribution from the $\Xi_{pq}(A\rightarrow B;S'M')$ CT states with $M_L=0$ to the $J_\perp$ exchange parameter.

Consider now the contributions from the $\Xi_{pq}(A\rightarrow B;S'M')$ CT states with $M_L=\pm1$, the cases (c) and (d). Combining two contributions (38) and (39) from the $M_L=1$ and $M_L=-1$ CT states and taking into account Eq. (42), we obtain the contribution to the diagonal matrix element

$$x_1(p,q)+y_1(p,q)mM_s, \tag{51}$$

where

$$x_1(p,q)=-\frac{C(p,q)^2}{E_{pq}(A\rightarrow B)}S, \tag{52a}$$

$$y_1(p,q)=-\frac{2C(p,q)^2}{E_{pq}(A\rightarrow B)}. \tag{52b}$$

This means that, in contrast to CT states with $M_L=0$, the contributions to J_z from $\Xi_{pq}(A\rightarrow B;S'M')$ CT states with $M_L=\pm1$ are always negative (antiferromagnetic). It is also important, that these CT states give no contribution to the nondiagonal matrix elements and thus to the $J_\perp$ exchange parameter.

Now we turn to the case of $S'=S+\frac{1}{2}$. Again, there are four types of contributions

(a′) $S'=S+\frac{1}{2},M'=M_s+\frac{1}{2}$, and $\Xi_{pq}(A\rightarrow B;S'M')\in M_L=0$;

$$\langle+\tfrac{1}{2},M_s|H_{AB}|\Xi_{pq}(A\rightarrow B;S'M')\rangle=A_1(p,q)\sqrt{S+M_s+1}, \tag{53}$$

(b′) $S'=S+\frac{1}{2},M'=M_s-\frac{1}{2}$, and $\Xi_{pq}(A\rightarrow B;S'M')\in M_L=0$;

$$\langle-\tfrac{1}{2},M_s|H_{AB}|\Xi_{pq}(A\rightarrow B;S'M')\rangle=B_1(p,q)\sqrt{S-M_s+1}, \tag{54}$$

(c′) $S'=S+\frac{1}{2},M'=M_s+\frac{1}{2}$, and $\Xi_{pq}(A\rightarrow B;S'M')\in M_L=+1$;

$$\langle-\tfrac{1}{2},M_s|H_{AB}|\Xi_{pq}(A\rightarrow B;S'M')\rangle=C_1(p,q)\sqrt{S+M_s+1}, \tag{55}$$

(d′) $S'=S+\frac{1}{2},M'=M_s-\frac{1}{2}$, and $\Xi_{pq}(A\rightarrow B;S'M')\in M_L=-1$;

$$\langle+\tfrac{1}{2},M_s|H_{AB}|\Xi_{pq}(A\rightarrow B;S'M')\rangle=D_1(p,q)\sqrt{S-M_s+1}. \tag{56}$$

As in cases (a)–(d), Eqs. (36)–(39), the factors $A_1(p,q)$, $B_1(p,q)$, $C_1(p,q)$, and $D_1(p,q)$ are related by $A_1(p,q)=\pm B_1(p,q)$ and $C_1(p',q')=\pm D_1(p,q)$. The contributions to J_z and $J_\perp$ are very similar to those in the previous case of $S'=S-\frac{1}{2}$ except that the signs of the contributions to J_z from CT states with $M_L=0$ and $M_L=\pm1$ are now opposite. In other words, in cases (a′) and (b′) the contribution to J_z is antiferromagnetic

$$x_2(p,q)+y_2(p,q)mM_s\Rightarrow\langle m,M_s|H_{\text{eff}}|m,M_s\rangle, \tag{57a}$$

$$x_2(p,q)=-\frac{A_1(p,q)^2}{E_{pq}(A\rightarrow B)}(S+1), \tag{57b}$$

$$y_2(p,q)=-\frac{2A_1(p,q)^2}{E_{pq}(A\rightarrow B)}, \tag{57c}$$

while in the cases (c′) and (d′) it is ferromagnetic

$$x_3(p,q)+y_3(p,q)mM_s\Rightarrow\langle m,M_s|H_{\text{eff}}|m,M_s\rangle, \tag{58a}$$

$$x_3(p,q)=-\frac{C_1(p,q)^2}{E_{pq}(A\rightarrow B)}(S+1), \tag{58b}$$

$$y_3(p,q)=+\frac{2C_1(p,q)^2}{E_{pq}(A\rightarrow B)}. \tag{58c}$$

The contribution to $J_\perp$ in the cases (a′) and (b′) is quite similar to that in the cases (a) and (b) for the spin $S'=S-\frac{1}{2}$ and is given by

$$\pm\frac{2C_1(p,q)^2}{E_{pq}(A\rightarrow B)}\Rightarrow J_\perp . \tag{59}$$

Depending on the angular part of $\Xi_{pq}(A\rightarrow B;S'M')$ CT wave functions with $M_L=0$, these contributions can be both ferro- and antiferromagnetic.

Contributions from the CT states of the $4f^{N+1}$-$3d^{M-1}$ configuration are treated similarly. These results show why the spin Hamiltonian describing the Yb^{3+}-Cr^{3+} superexchange in the $YbCrBr_9{}^{3-}$ dimer is strictly bilinear with respect to S_{Yb} and S_{Cr} spin operators, and why no higher powers in S_{Cr} appear.

D. Analysis of contributions from CT states to the exchange parameters of the $YbCrBr_9{}^{3-}$ dimer

It is of interest to analyze quantitatively the balance of contributions from individual states of the $4f^{12}$-$3d^4$ and $4f^{14}$-$3d^2$ configurations to the exchange parameters A_0, J_z, and $J_\perp$. This cannot be done analytically due to a very large number of CT states and a complicated orbital composition of their many-electron wave functions. Contributions from the $4f^{12}$-$3d^4$ configuration to the exchange parameters J_z and $J_\perp$ obtained from numerical calculations at $U_0(A\rightarrow B)=10$ eV are given in Table V in the order of increasing energy of CT states. Since the total number of individual contributions is too large (several thousands), the contributions from the $4f^{12}$-$3d^4$ CT configuration are summed over multiply degenerate levels of the $\Xi_{pq}(A\rightarrow B;S'M')=\Psi_p(4f^{12})\otimes\Phi_q(3d^4;S'M')$ states originating from various combinations the $2J+1$-fold degenerate $^{2S+1}L_J$ multiplets of the $4f^{12}$ configuration of ytterbium and those of the $^{2S+1}\Gamma_i$ CF levels of the $3d^4$ configuration of chromium (represented by $^{2S+1}A_{1g}$ and $^{2S+1}A_{2g}$ orbital singlets, $^{2S+1}E_g$ doublets, and $^{2S+1}T_{1g}$ and $^{2S+1}T_{2g}$ triplets).

A complicated interplay between numerous contributions can be seen from Table V. These contributions differ considerably in magnitude and have opposite signs. It is important to note that the absolute value of some individual contributions is comparable to or even larger than the net exchange parameters J_z and $J_\perp$; this is especially true for the small parameter J_z. These data show that in the general case the sign of exchange parameters cannot be rationalized in a simple way, since it is a result of a complicated competition between numerous ferromagnetic and antiferromagnetic contributions coming from various CT states, whose energies can differ considerably from each other. It is interesting that the main contribution to J_z or $J_\perp$ does not originate from one or few low-lying CT states, but many CT states contribute to the net exchange parameters. Even high-lying CT states give large contributions, such as the $^1I_6\otimes{}^3T_{1g}(1)$ state lying at 120 000 cm^{-1} [i.e., about 5 eV above the CT energy gap of $U_0(A\rightarrow B)=10$ eV]. Table V show, that the sum of contributions approaches to the net exchange parameter only for energies larger than 123 000 cm^{-1}; a value about 1.5 times larger than the CT energy gap $U_0(A\rightarrow B)=80\,650$ cm^{-1} (10 eV). We can therefore conclude, that the total balance of contributions to J_z and $J_\perp$ is very sensitive to the CT energies. This implies, in particular, that the widely used approximation, according to which all CT states are assumed to have the constant energy U, can lead to considerable errors for $4f$-$3d$ exchange systems. Indeed, calculations with constant CT energies $E_{pq}(A\rightarrow B)\equiv 10$ eV and $E_{rs}(A\leftarrow B)\equiv 5$ eV yield $J_z=-2.36$, $J_\perp=-0.16$ cm^{-1} for the $4f^{12}$-$3d^4$ configuration and $J_z=-4.71$, $J_\perp=-0.33$ cm^{-1} for the $4f^{14}$-$3d^2$ configuration. The total result $J_z=-7.07$, $J_\perp=-0.49$ cm^{-1} differs greatly from the above result obtained with actual CT energies, $J_z=-4.95$, $J_\perp=+4.06$ cm^{-1} (Table IV). Although the strong exchange anisotropy retains, the ratio between J_z and $J_\perp$ parameters becomes quite different: the parameter $J_\perp$ reduces dramatically and reverses the sign in going from the actual to constant CT energies.

Interestingly that, although the two contributions to J_z, and $J_\perp$ from the group of degenerate CT states with the same energy correlate to each other, they are far from being simply proportional, Table V. This is consistent with the conclusions of the previous paragraph. A very large negative value of the spin-independent parameter A_0 (Table IV) can also be rationalized in terms of Eqs. (36)–(58). Indeed, according to Eqs. (46), (52), and (57), each individual CF state contributing to the J_z parameter gives a comparable contribution to A_0; the latter is always negative while the contributions to J_z have different signs and thus they almost cancel each other, as can be seen from Table V.

Of the $^{2S+1}\Gamma_i$ states of the $4d^4$ configuration, only ^5E_g, ^3E_g, and $^3T_{1g}$ states are contributive to the exchange parameters; in Fig. 4 they are enumerated and marked by star. By contrast, all $^{2S+1}L_J$ states of the $4f^{12}$ configuration of ytterbium are contributive. The distribution of the contributions to the J_z and $J_\perp$ exchange parameters over the energy levels of the $4f^{12}$ and $3d^4$ configurations are presented in Tables VI and VII. The general character of the distribution is quite different for $4f$ and $3d$ states: while even high-lying multiplets of the $4f^{12}$ configuration (such as the $^3P_2$ multiplet at 38 000 cm^{-1}) may give considerable contributions to J_z and $J_\perp$, the main fraction of the total contribution to the exchange parameters originate from the low-lying $^{2S+1}\Gamma_i$ states of the $3d^4$ configuration. This observation can serve as a good illustration of the well-known fact that the correlation effects in the open $4f$ shell are generally more pronounced than those in the $3d$ shell due to a small radial extension of the $4f$ states and their large orbital momentum.

With the $4f^{14}$-$3d^2$ CT configuration we are in a much more comfortable situation because the ytterbium center has the closed $4f^{14}$ shell. This means that the energy structure of this CT configuration coincides with that of the $3d^2$ configuration of the chromium center. This fact can be used to illustrate the microscopic origin of the exchange anisotropy in more detail. Table VIII shows that the contributions to J_z and $J_\perp$ come only from the two triplet states of the $3d^2$ configuration $^3T_{1g}(1)$ and $^3T_{1g}(2)$.

TABLE V. Contributions to the J_z and $J_\perp$ exchange parameters from the $\Xi_{pq}(A\rightarrow B;S'M')=\Psi_p(4f^{12})\otimes\Phi_q(3d^4;S'M')$ individual states of the $4f^{12}$-$3d^4$ CT configuration in the $YbCrBr_9^{3-}$ dimer. All energies are given in cm^{-1}.

$\Psi_p(4f^{12})\otimes\Phi_q(3d^4)$ CT states[a]					Contributions to the J_z and $J_\perp$ parameters[c]			
Yb $4f^{12}$		Cr $4d^4$		$E_{pq}(A\rightarrow B)$[b]				
$^{2S+1}L_J$	$E_p(^{2S+1}L_J)$	$^{2S+1}\Gamma_i$	$E_q(^{2S+1}\Gamma_i)$		J_z[d]	$\sum J_z$[e]	$J_\perp$[d]	$\sum J_\perp$[e]
$^3H_6$	0	^5E_g	0	80650	−0.491	−0.491	−2.451	−2.451
$^3H_6$	0	$^3T_{1g}(1)$	4772	85422	+11.021	+10.530	+24.233	+21.782
$^3F_4$	5610	^5E_g	0	86260	+0.775	+11.304	+0.072	+21.854
$^3H_5$	8188	^5E_g	0	88838	+0.091	+11.395	+0.705	+22.559
$^3F_4$	5610	$^3T_{1g}(1)$	4772	91031	−8.134	+3.261	−1.851	+20.708
$^3H_4$	12518	^5E_g	0	93168	−0.598	+2.663	−0.645	+20.063
$^3H_5$	8188	$^3T_{1g}(1)$	4772	93609	−3.977	−1.314	−7.943	+12.120
$^3F_3$	14308	^5E_g	0	94958	+0.975	−0.338	+0.229	+12.350
$^3F_2$	14914	^5E_g	0	95564	−0.544	−0.883	+0.742	+13.092
$^3H_6$	0	$^3E_g(1)$	15476	96126	+0.258	−0.624	+1.290	+14.382
$^3H_4$	12518	$^3T_{1g}(1)$	4772	97940	+4.416	+3.829	+4.263	+18.730
$^3F_3$	14308	$^3T_{1g}(1)$	4772	99729	−2.336	+1.493	+3.330	+22.060
$^3F_2$	14914	$^3T_{1g}(1)$	4772	100336	+1.044	+2.538	−8.908	+13.152
$^3F_4$	5610	$^3E_g(1)$	15476	101735	−0.412	+2.126	−0.038	+13.114
$^3H_6$	0	$^3E_g(2)$	21118	101768	+0.144	+2.270	+0.721	+13.834
$^1G_4$	21172	^5E_g	0	101822	+0.072	+2.342	−0.038	+13.796
$^3H_5$	8188	$^3E_g(1)$	15476	104313	−0.049	+2.265	−0.377	+13.412
$^3H_6$	0	$^3T_{1g}(3)$	25907	106557	+0.075	+2.326	+0.165	+13.550
$^1G_4$	21172	$^3T_{1g}(1)$	4772	106594	−0.501	+1.825	+0.258	+13.809
$^3F_4$	5610	$^3E_g(2)$	21118	107378	−0.231	+1.594	−0.021	+13.787
$^1D_2$	27830	^5E_g	0	108480	−0.899	+0.696	+0.298	+14.085
$^3H_4$	12518	$^3E_g(1)$	15476	108644	+0.322	+1.017	+0.347	+14.432
$^3H_5$	8188	$^3E_g(2)$	21118	109956	−0.027	+1.006	−0.211	+14.236
$^3F_3$	14308	$^3E_g(1)$	15476	110433	−0.526	+0.480	−0.124	+14.112
$^3F_2$	14914	$^3E_g(1)$	15476	111040	+0.294	+0.774	−0.401	+13.711
$^1D_2$	27830	$^3T_{1g}(1)$	4772	113251	+6.288	+7.001	−2.309	+11.370
$^3H_4$	12518	$^3E_g(2)$	21118	114286	+0.181	+7.182	+0.195	+11.568
$^1I_6$	34684	^5E_g	0	115334	+0.983	+8.138	+0.865	+12.378
$^3F_3$	14308	$^3E_g(2)$	21118	116076	−0.296	+7.842	−0.069	+12.309
$^3F_2$	14914	$^3E_g(2)$	21118	116682	+0.165	+8.043	−0.225	+12.083
$^3P_1$	36096	^5E_g	0	116746	+0.170	+8.213	+0.104	+12.187
$^3P_2$	37991	^5E_g	0	118641	−0.367	+7.810	−0.373	+11.847
$^1I_6$	34684	$^3T_{1g}(1)$	4772	120106	−9.006	−1.166	−8.132	+3.745
$^3P_0$	35435	$^3T_{1g}(1)$	4772	120857	−0.242	−1.408	−0.017	+3.728
$^3P_1$	36096	$^3T_{1g}(1)$	4772	121517	−1.258	−2.675	−0.748	+2.941
$^3P_2$	37991	$^3T_{1g}(1)$	4772	123413	+2.479	−0.221	+2.253	+5.204
$^1D_2$	27830	$^3E_g(1)$	15476	123955	+0.493	+0.272	−0.164	+5.040
$^3H_6$	0	$^3T_{1g}(6)$	46050	126700	+0.151	+0.443	+0.331	+5.361
$^1D_2$	27830	$^3E_g(2)$	21118	129598	+0.279	+0.718	−0.093	+5.268
$^1I_6$	34684	$^3E_g(1)$	15476	130810	−0.544	+0.177	−0.478	+4.792
$^3F_4$	5610	$^3T_{1g}(6)$	46050	132309	−0.113	−0.083	−0.026	+4.677
$^3H_6$	0	$^3T_{1g}(7)$	52264	132914	+0.061	−0.023	+0.133	+4.810
$^3P_2$	37991	$^3E_g(1)$	15476	134117	+0.204	+0.175	+0.207	+5.014
$^3H_5$	8188	$^3T_{1g}(6)$	46050	134887	−0.056	+0.165	−0.112	+4.886
$^1I_6$	34684	$^3E_g(2)$	21118	136452	−0.308	−0.134	−0.271	+4.623

TABLE V. *(Continued).*

$\Psi_p(4f^{12})\otimes\Phi_q(3d^4)$ CT states[a]								
Yb $4f^{12}$		Cr $4d^4$		$E_{pq}(A\rightarrow B)$[b]	Contributions to the J_z and $J_\perp$ parameters[c]			
$^{2S+1}L_J$	$E_p(^{2S+1}L_J)$	$^{2S+1}\Gamma_i$	$E_q(^{2S+1}\Gamma_i)$		J_z[d]	$\sum J_z$[e]	$J_\perp$[d]	$\sum J_\perp$[e]
$^3P_2$	37991	$^3E_g(2)$	21118	139759	+0.116	−0.066	+0.117	+4.758
$^3F_2$	14914	$^3T_{1g}(6)$	46050	141614	+0.015	−0.171	−0.128	+4.573
$^1D_2$	27830	$^3T_{1g}(6)$	46050	154530	+0.093	−0.066	−0.034	+4.541
$^1I_6$	34684	$^3T_{1g}(6)$	46050	161384	−0.136	−0.148	−0.122	+4.406
$^1S_0$	79390	$^3T_{1g}(1)$	4772	164812	−0.100	−0.233	−0.007	+4.421
				Total:		$J_z=-0.299$		$J_\perp=+4.381$

[a]Contributions to the J_z and $J_\perp$ exchange parameters are summed over multiply degenerate $\Xi_{pq}(A\rightarrow B;S'M')=\Psi_p(4f^{12})\otimes\Phi_q(3d^4;S'M')$ CT states originating from various combinations the $2J+1$-fold degenerate $^{2S+1}L_J$ multiplets of the $4f^{12}$ configuration of Yb and $^{2S+1}\Gamma_i$ crystal-field levels (^5E_g, ^3E_g, or $^3T_{1g}$) of the $3d^4$ configuration of Cr.
[b]$E_{pq}(A\rightarrow B)=U_0(A\rightarrow B)+E_p(^{2S+1}L_J)+E_q(^{2S+1}\Gamma_i)$, where $U_0(A\rightarrow B)=80650\ \mathrm{cm}^{-1}$ (10 eV).
[c]The sign of J_z and $J_\perp$ corresponds to the true sign of the exchange parameters (see the text for detail).
[d]Contributions, in which both J_z and $J_\perp$ are less than 0.1 cm^{-1} are not shown.
[e]The sum of contributions to J_z and $J_\perp$ parameters from the CT states with the energy less than or equal to $E_{pq}(A\rightarrow B)$.

The main contribution originates from the ground $^3T_{1g}(1)$ state, and a considerably smaller contribution comes from the excited $^3T_{1g}(2)$ state (marked by star in Fig. 4) lying at 21 049 cm^{-1} above the ground state. Note that the contributions to J_z and $J_\perp$ originate from different individual states of the ground triply degenerate $^3T_{1g}$ level, which are also shown in Table VIII. It is interesting to compare the wave function (30) of the ground $^4A_{2g}$ state of $Cr^{3+}(3d^3)$ ion

$$\frac{\sqrt{2}}{3}\{\mathrm{Det}(d_2\alpha,d_1\alpha,d_0\alpha)-\mathrm{Det}(d_0\alpha,d_{-1}\alpha,d_{-2}\alpha)\}+\frac{2}{3}\mathrm{Det}(d_2\alpha,d_0\alpha,d_{-2}\alpha)+\frac{1}{3}\mathrm{Det}(d_1\alpha,d_0\alpha,d_{-1}\alpha),$$

and the wave functions of the triply degenerate $^3T_{1g}(1,M_L)$ ground state of $Cr^{4+}(3d^2)$ ion (where $M_L=0,\pm1$ is the pro-

TABLE VI. The distribution of contributions to the J_z and $J_\perp$ exchange parameters over the $^{2S+1}L_J$ multiplets of the $4f^{12}$ configuration of Yb (the contributions for the given $^{2S+1}L_J$ multiplet of the $4f^{12}$ configuration of ytterbium are summed over $^{2S+1}\Gamma_i$ states of the $3d^4$ configuration of chromium). All energies are given in cm^{-1}.

$^{2S+1}L_J$	$E(^{2S+1}L_J)$	J_z	$\sum J_z$[a]	$J_\perp$	$\sum J_\perp$[a]
$^3H_6$	0	+11.263	+11.263	+24.520	+24.520
$^3F_4$	5610	−8.251	+3.012	−1.895	+22.625
$^3H_5$	8188	−4.084	−1.072	−8.070	+14.555
$^3H_4$	12518	+4.458	+3.386	+4.293	+18.848
$^3F_3$	14308	−2.257	+1.129	+3.470	+22.318
$^3F_2$	14914	+0.993	+2.122	−9.071	+13.247
$^1G_4$	21172	−0.507	+1.615	+0.261	+13.508
$^1D_2$	27830	+6.365	+7.980	−2.341	+11.167
$^1I_6$	34684	−9.169	−1.189	−8.282	+2.885
$^3P_0$	35435	−0.245	−1.434	−0.017	+2.868
$^3P_1$	36096	−1.277	−2.711	−0.758	+2.110
$^3P_2$	37991	+2.513	−0.198	+2.278	+4.388
$^1S_0$	79390	−0.101	−0.299	−0.007	+4.381
		Total:	$J_z=-0.299$		$J_\perp=+4.381$

[a]The sum of contributions to J_z and $J_\perp$ parameters from the $^{2S+1}L_J$ multiplets with the energy less than or equal to $E(^{2S+1}L_J)$.

TABLE VII. The distribution of contributions to the J_z and $J_\perp$ exchange parameters over the $^{2S+1}\Gamma_i$ states of the $3d^4$ configuration of chromium (the contributions for the given $^{2S+1}\Gamma_i$ energy level of the $3d^4$ configuration of chromium are summed over the $^{2S+1}L_J$ multiplets of the $4f^{12}$ configuration of ytterbium). All energies are given in cm^{-1}.

$^{2S+1}\Gamma_i$	$E(^{2S+1}\Gamma_i)$	J_z	$\sum J_z$ [b]	$J_\perp$	$\sum J_\perp$ [b]
^5E_g	0	+0.2172	+0.2172	−0.4903	−0.4903
$^3T_{1g}(1)$	4772	−0.3053	−0.0881	+4.4241	+3.9339
$^3E_g(1)$	15476	−0.1208	−0.2089	+0.2251	+4.1589
$^3T_{1g}(2)$	16286	−0.0016	−0.2105	+0.0138	+4.1727
$^3E_g(2)$	21118	−0.0686	−0.2791	+0.1201	+4.2928
$^3T_{1g}(3)$	25907	−0.0040	−0.2832	+0.0252	+4.3181
$^3T_{1g}(4)$	28901	−0.00002	−0.2832	+0.00005	+4.3181
$^3E_g(3)$	32706	−0.0003	−0.2835	+0.0005	+4.3186
$^3T_{1g}(5)$	36521	−0.0003	−0.2838	+0.0015	+4.3201
$^3T_{1g}(6)$	46050	−0.0107	−0.2945	+0.0436	+4.3637
$^3T_{1g}(7)$	52264	−0.0046	−0.2991	+0.0169	+4.3806
		Total:[b]	$J_z=-0.2991$		$J_\perp=+4.3806$

[a]The sum of contributions to J_z and $J_\perp$ parameters from the $^{2S+1}\Gamma_i$ energy levels with the energy less than or equal to $E(^{2S+1}\Gamma_i)$.
[b]The sign of J_z and $J_\perp$ corresponds to the true sign of the exchange parameters (see the text for detail).

jection of the quasimomentum $L=1$) in the octahedral ligand surrounding

$$^3T_{1g}(1,M_L=0)=0.510\{\mathrm{Det}(d_2\alpha,d_1\alpha)-\mathrm{Det}(d_{-1}\alpha,d_{-2}\alpha)\}+0.517\mathrm{Det}(d_2\alpha,d_{-2}\alpha)+0.462\mathrm{Det}(d_1\alpha,d_{-1}\alpha), \quad (60a)$$

$$^3T_{1g}(1,M_L=-1)=0.144\mathrm{Det}(d_1\alpha,d_{-2}\alpha)+0.448\mathrm{Det}(d_0\alpha,d_{-1}\alpha)+0.882\mathrm{Det}(d_2\alpha,d_0\alpha), \quad (60b)$$

$$^3T_{1g}(1,M_L=+1)=-0.144\mathrm{Det}(d_2\alpha,d_{-1}\alpha)-0.448\mathrm{Det}(d_1\alpha,d_0\alpha)+0.882\mathrm{Det}(d_0\alpha,d_{-2}\alpha). \quad (60c)$$

The ground $^3T_{1g}(1)$ level of $Cr^{4+}(3d^2)$ is predominantly (96%) represented by the $(t_{2g})^2$ configuration, which differs by one t_{2g} electron from the pure $(t_{2g})^3$ configuration of the $^4A_{2g}$ ground level of $Cr^{3+}(3d^3)$. Since the orbital part of the $^3T_{1g}(1,M_L)$ state transforms as the momentum $L=1$ with the projection M_L upon rotations around the C_3 axis by the angles $\pm 2\pi/3$, in accordance to the rules established above, Eqs. (46), (50), and (52), only the $^3T_{1g}(1,M_L=0)$ state contribute to the $J_\perp$ exchange parameter, while contributions to J_z come from both the $^3T_{1g}(1,M_L=0)$ state and $^3T_{1g}(1,M_L=\pm 1)$ states (Table VIII).

This comparison between the orbital composition of the $|\Gamma_{6,}m\rangle$ wave functions (29) and that of the wave functions (30) and (60) is helpful in elucidating the origin of the J_z exchange parameter and its sign. According to Table VIII, the $^3T_{1g}(1,M_L=-1)$ and $^3T_{1g}(1,M_L=+1)$ states give the largest contribution to J_z. In the C_{3v} group they refer to the

TABLE VIII. Contributions to the J_z and $J_\perp$ exchange parameters from the $\Xi_{rs}(A\leftarrow B)=\Psi_r(4f^{14})\otimes\Phi_s(3d^2)$ states of the $4f^{14}$-$3d^2$ CT configuration in the $YbCrBr_9^{3-}$ dimer [since the ytterbium center has the $4f^{14}$ closed-shell configuration represented by the only state, the index r at $\Xi_{rs}(A\leftarrow B)=\Psi_r(4f^{14})\otimes\Phi_s(3d^2)$ can be omitted]. All energies are given in cm^{-1}.

Cr $4d^2$		$E_{rs}(A\leftarrow B)$[a]	$\Psi_r(4f^{14})\otimes\Phi_s(3d^2)$ CT states: Contributions to the J_z and $J_\perp$ parameters[b]			
$^{2S+1}\Gamma_i$	$E_s(^{2S+1}\Gamma_i)$		J_z	$\sum J_z$ [c]	$J_\perp$	$\sum J_\perp$ [c]
$^3T_{1g}(1,M_L=0)$	0	40325	+0.3125	+0.3125	−0.3125	−0.3125
$^3T_{1g}(1,M_L=\pm 1)$	0	40325	−4.8323	−4.5198	0	−0.3125
$^3T_{1g}(2,M_L=0)$	21049	61384	+0.0088	−4.5110	−0.0088	−0.3213
$^3T_{1g}(2,M_L=\pm 1)$	21049	61384	−0.1376	−4.6486	0	−0.3213
			Total:	$J_z=-4.6486$		$J_\perp=-0.3213$

[a]$E_s(A\leftarrow B)=U_0(A\leftarrow B)+E_s(^{2S+1}\Gamma_i)$, where $U_0(A\leftarrow B)=40\,325\ cm^{-1}$ (5 eV).
[b]The sign of J_z and $J_\perp$ corresponds to the true sign of the exchange parameters (see the text for detail).
[c]The sum of contributions to J_z and $J_\perp$ parameters from the CT states with the energy less than or equal to $E_s(A\leftarrow B)$.

E representation, cases (c) and (d) [Eqs. (36) and (37)]. The ${}^3T_{1g}(1,M_L=-1)$ and ${}^3T_{1g}(1,M_L=+1)$ states with the spin projection M_s contribute, respectively, to the $\langle -\frac{1}{2},M_s|H_{\rm eff}|-\frac{1}{2},M_s\rangle$ [case (c)] and $\langle +\frac{1}{2},M_s|H_{\rm eff}|+\frac{1}{2},M_s\rangle$ [case (d)] diagonal matrix elements. Consider the contribution to the $\langle +\frac{1}{2},\frac{3}{2}|H_{\rm eff}|+\frac{1}{2},\frac{3}{2}\rangle$ diagonal matrix element coming from the ${}^3T_{1g}(1,M_L=+1)$ state (60c), which is predominantly presented by the $\mathrm{Det}(d_0\alpha,d_{-2}\alpha)$ determinant. This contribution refers to the case (c), $S'=S-\frac{1}{2}$, $M'=M_s-\frac{1}{2}$, and $\Xi_{pq}(A\leftarrow B;S'M')\in M_L=+1$ [Eq. (38)]. As can be seen from the comparison between the composition of ${}^3T_{1g}(1,M_L=+1)$ and that of the wave function (30) of the ground ${}^4A_{2g}$ state of $Cr^{3+}(3d^3)$, the $\langle +\frac{1}{2},\frac{3}{2}|H_{AB}|(4f^{14})\otimes[{}^3T_{1g}(1,M_L=+1);S'=1,M'=1]\rangle$ matrix element originates mainly due to the $4f\leftarrow 3d$ transfer, in which an electron moves from the $d_2\alpha$ or $d_{-1}\alpha$ orbital; the transfer from the $d_0\alpha$ orbital is less important since the coefficient at the $\mathrm{Det}(d_2\alpha,d_{-1}\alpha)$ determinant in ${}^3T_{1g}(1,M_L=+1)$ [Eq. (60c)] is much smaller. The $d_2\alpha$ or $d_{-1}\alpha$ orbitals are connected to the $4f_2\alpha$ orbital of ytterbium [which is presented with a maximum weight of $\sqrt{30/54}$ in the $|\Gamma_{6,}+\frac{1}{2}\rangle$ wave function (29)] via the nonzero transfer integrals t_{22} and t_{-12} (Table III); in other words, an electron moves from the $d_{-1}\alpha$ or $d_2\alpha$ orbital on Cr^{3+} to fill the $[4f_2\alpha]$ hole on Yb^{3+} and to make the closed $4f^{14}$ shell. Other $4f_i\alpha\leftarrow 3d_j\alpha$ electron transfers with $i-j=0$ or ± 3 are of minor importance due to much smaller coefficients at the determinants, which are connected by these transfers. Numerical values of the $\langle +\frac{1}{2},M_s|H_{AB}|(4f^{14})\otimes[{}^3T_{1g}(1,M_L=+1);M'=M_s-1]\rangle$ matrix elements are

$$\langle +\tfrac{1}{2},\tfrac{3}{2}|H_{AB}|(4f^{14})\otimes[{}^3T_{1g}(1,M_L=+1);M'=1]\rangle = -540.65\ \mathrm{cm}^{-1}, \tag{61a}$$

$$\langle +\tfrac{1}{2},\tfrac{1}{2}|H_{AB}|(4f^{14})\otimes[{}^3T_{1g}(1,M_L=+1);M'=0]\rangle = -441.43\ \mathrm{cm}^{-1}, \tag{61b}$$

$$\langle +\tfrac{1}{2},-\tfrac{1}{2}|H_{AB}|(4f^{14})\otimes[{}^3T_{1g}(1,M_L=+1);M'=-1]\rangle = -311.97\ \mathrm{cm}^{-1}, \tag{61c}$$

which are proportional to $\sqrt{S+M_s}$ (with $S=\frac{3}{2}$), as predicted by the Eq. (38), case (c); the matrix element for the $\langle +\frac{1}{2},-\frac{3}{2}|$ state is zero because the $|[{}^3T_{1g}(1,M_L=1);M'=-2]\rangle$ state does not exist. Similarly for the $\langle -\frac{1}{2},M_s|H_{AB}|(4f^{14})\otimes[{}^3T_{1g}(1,M_L=-1);M']\rangle$ matrix elements, which obey the relationships $\langle -\frac{1}{2},-M_s|H_{AB}|(4f^{14})\otimes[{}^3T_{1g}(1,M_L=-1);-M']\rangle=\langle +\frac{1}{2},M_s|H_{AB}|(4f^{14})\otimes[{}^3T_{1g}(1,M_L=+1);M']\rangle$.

From a similar consideration one can also realize that the $\langle -\frac{1}{2},\frac{3}{2}|H_{AB}|(4f^{14})\otimes[{}^3T_{1g}(1,M_L=+1);M']\rangle$ and $\langle +\frac{1}{2},\frac{3}{2}|H_{AB}|(4f^{14})\otimes[{}^3T_{1g}(1,M_L=-1);M']\rangle$ matrix elements are strictly zero. Therefore, according to Eqs. (51) and (52), the contribution from the ${}^3T_{1g}(1,M_L=-1)$ and ${}^3T_{1g}(1,M_L=+1)$ states to the exchange spin Hamiltonian is given by $x_1(p,q)+y_1(p,q)mM_s$, where $y_1(p,q)=-4.8323\ \mathrm{cm}^{-1}$ is the contribution to J_z determined by Eq. (52b) (Table VIII). The antiferromagnetic sign of J_z is clearly seen from Eq. (61), which shows that the $\langle +\frac{1}{2},\frac{3}{2}|H_{AB}|(4f^{14})\otimes[{}^3T_{1g}(1,M_L=+1);M'=1]\rangle$ matrix element is the largest one, and thus the state $|+\frac{1}{2},\frac{3}{2}\rangle$ with the parallel orientation of the effective spin $S=\frac{1}{2}$ of Yb^{3+} and true spin $S=\frac{3}{2}$ of Cr^{3+} (and, respectively, with the antiparallel orientation of their magnetic moments) have the lowest energy among $|+\frac{1}{2};M_s\rangle$ states.

Similar analysis show that for the ${}^3T_{1g}(1,M_L=0)$ state the $\langle +\frac{1}{2},M_s|H_{AB}|(4f^{14})\otimes[{}^3T_{1g}(1,M_L=0);M'=M_s+\frac{1}{2}]\rangle$ and $\langle -\frac{1}{2},M_s|H_{AB}|(4f^{14})\otimes[{}^3T_{1g}(1,M_L=0);M'=M_s-\frac{1}{2}]\rangle$ matrix elements are nonzero. As can be seen from the orbital composition of the wave function ${}^3T_{1g}(1,M_L=0)$, Eq. (60a), an electron can move from the $d_0\alpha$ orbital only and thus it can arrive at the $f_0\alpha$ orbital or $f_{\pm 3}\alpha$ orbital, which are represented in the wave functions $|\Gamma_{6,}m\rangle$ (29) with rather small weights ($\sqrt{8/54}$ and $\sqrt{5/54}$, respectively). As a result, these matrix elements are considerably smaller

$$\langle +\tfrac{1}{2},\tfrac{1}{2}|H_{AB}|(4f^{14})\otimes[{}^3T_{1g}(1,M_L=0);M'=1]\rangle = \langle -\tfrac{1}{2},-\tfrac{1}{2}|H_{AB}|(4f^{14})\otimes[{}^3T_{1g}(1,M_L=0);M'=-1]\rangle = 79.37\ \mathrm{cm}^{-1}, \tag{62a}$$

$$\langle +\tfrac{1}{2},-\tfrac{1}{2}|H_{AB}|(4f^{14})\otimes[{}^3T_{1g}(1,M_L=0);M'=0]\rangle = \langle -\tfrac{1}{2},\tfrac{1}{2}|H_{AB}|(4f^{14})\otimes[{}^3T_{1g}(1,M_L=0);M'=0]\rangle = 112.25\ \mathrm{cm}^{-1}, \tag{62b}$$

$$\langle +\tfrac{1}{2},-\tfrac{3}{2}|H_{AB}|(4f^{14})\otimes[{}^3T_{1g}(1,M_L=0);M'=-1]\rangle = \langle -\tfrac{1}{2},\tfrac{3}{2}|H_{AB}|(4f^{14})\otimes[{}^3T_{1g}(1,M_L=0);M'=1]\rangle = 137.48\ \mathrm{cm}^{-1}. \tag{62c}$$

Correspondingly, the contributions to J_z from the ${}^3T_{1g}(1,M_L=0)$ state are considerably smaller than those from the ${}^3T_{1g}(1,M_L=-1)$ and ${}^3T_{1g}(1,M_L=+1)$ states. In contrast to the previous case, this contribution is ferromagnetic being consistent with the cases (a) and (b), Eqs. (36) and (37). Indeed, an electron moves from the $d_0\alpha$ orbital of the ${}^4A_{2g}(M_s=\frac{3}{2})$ wave function to the $f_0\alpha$ or $f_{\pm 3}\alpha$ orbital which is contained in the $|\Gamma_{6,}-\frac{1}{2}\rangle$ wave function, but is not contained in the $|\Gamma_{6,}+\frac{1}{2}\rangle$ wave function. Therefore, the $|-\frac{1}{2},\frac{3}{2}\rangle$ state with the antiparallel orientations of spins (and with the parallel orientation of the magnetic moments) is stabilized due to the contribution described by Eq. (46), while the $|+\frac{1}{2},\frac{3}{2}\rangle$ state is not stabilized. Note that, in contrast to the ${}^3T_{1g}(1,M_L=-1)$ and ${}^3T_{1g}(1,M_L=+1)$ states, the ${}^3T_{1g}(1,M_L=0)$ state contributes to $J_\perp$. Indeed, since the $|m,M_s\rangle$ and $|m-1,M_s+1\rangle$ states are connected to the same ${}^3T_{1g}(1,M_L=0)$ CT state with the spin projection $M'=M_s+m$ via the nonzero matrix elements, Eqs. (36) and (37), the $\langle m,M_s|H_{\rm eff}|m-1,M_s+1\rangle$ nondiagonal matrix elements are nonzero, which are directly related to the $J_\perp$ parameter, Eqs. (47)–(50).

The analysis of contributions from the excited ${}^3T_{1g}(2)$ level at 21 049 cm^{-1} is quite similar to that for the ground ${}^3T_{1g}(1)$ level. However, since this state is predominantly represented by the $(t_{2g}e_g)$ configuration, its contribution almost vanishes due to the orthogonality of t_{2g} and e_g3d or-

bitals centered on the Cr^{3+} ion; some nonzero contributions arise because of a small (about 4%) admixture of the $(t_{2g})^2$ configuration (Table VIII).

Our results indicate that the $4f$-$3d$ superexchange interaction may be strongly anisotropic even if the CF anisotropy of the exchange-coupled magnetic ions is completely vanishing. Indeed, the exchange spin Hamiltonian $H_{4f\text{-}3d}$ [Eq. (33)] of the $YbCrBr_9^{3-}$ dimer is extremely anisotropic (in which the J_z and $J_\perp$ exchange parameters even have opposite signs) despite the fact that the Γ_6 ground state of the Yb^{3+} ion in the regular $YbBr_6^{3-}$ octahedron is magnetically isotropic. The same is especially true for the Cr^{3+} ion, whose ground-state total spin $S_{Cr}=\frac{3}{2}$ is a good quantum number (since the spin-orbit coupling for $3d$ electrons or zero-field splitting of the $^4A_{2g}$ ground state were not taken into account in our approach). We can therefore conclude that, although it is commonly believed in the literature that the exchange anisotropy in lanthanide compounds is closely related to the single-ion magnetic anisotropy of lanthanide ions, strong exchange anisotropy is an immanent property of the $4f$-$3d$ superexchange interaction, which is not necessarily related to the CF anisotropy. Similar results were previously obtained for other lanthanide exchange-coupled pairs, such as $Ln^{3+}M^{n+}L_{11}$ bioctadedral corner-sharing model dimers (where $Ln^{3+}=Ce^{3+}$ or Yb^{3+}, $M^{n+}=Cr^{3+}$, Mn^{2+}, or Ni^{2+})[35] or bioctadedral corner-and edge-sharing f^1-f^1 dimers.[19] However, in $4f$-$3d$ dimers with a lower symmetry of the ligand surrounding around the lanthanide ion, both the exchange anisotropy and CF anisotropy should be taken in account.

Although the $4s$(Br) states give smaller contributions to the transfer integrals than the $4p$(Br) states do (Table III), their taking into account is important for a correct analysis of $4f$-$3d$ exchange interactions. Calculations performed with various combinations of transfer integrals show that the J_z and $J_\perp$ exchange parameters are not additive neither with respect to the $4p$(Br) and $4s$(Br) contributions to the transfer integrals, nor with respect to σ and π $4f$-$3d$ superexchange pathways.

In our study we tried to establish general principles of the superexchange interaction between lanthanide and transition metal ions and to understand the microscopic origin of a strong $4f$-$3d$ superexchange anisotropy. For this reason we used a simplified model that includes only the most important interactions. In particular, we did not take into account electron transfers from half-filled $3d$(Cr) orbitals to empty $5d$(Yb) orbitals whose influence on the exchange parameters may also be important.[19] Further development of the $4f$-$3d$ superexchange theory requires more accurate determining the key parameters, especially the transfer integrals and CT energy gaps in exchange systems involving lanthanide ions.

V. SUMMARY AND CONCLUSIONS

The main purpose of this paper has been to analyze quantitatively the microscopic mechanism of the exchange interaction between Yb^{3+} and Cr^{3+} ions in the $YbCrBr_9^{3-}$ bioctahedral face-sharing dimer and, especially, to establish the origin of an extremely strong exchange anisotropy. To this end, a new form of the superexchange theory has been used which is specially adapted for an adequate description of a complicated electronic structure of lanthanide ions in solids and for a direct calculation of the $4f$-$3d$ exchange parameters. The spin Hamiltonian of the Yb^{3+}-Cr^{3+} superexchange interaction obtained from numerical parametric calculations is found to be extremely anisotropic, $H_{4f\text{-}3d}=J_z S^z_{Yb}S^z_{Cr}+J_\perp(S^x_{Yb}S^x_{Cr}+S^y_{Yb}S^y_{Cr})$, in which the exchange parameters have opposite signs ($J_z<0$ and $J_\perp>0$) in the whole range of CT energies (Fig. 5). The exchange parameters $J_z=-4.95$ and $J_\perp=+4.06\ cm^{-1}$ calculated at the CT energies $U_0(A\rightarrow B)=10$ and $U_0(A\leftarrow B)=5$ eV (estimated from the redox potentials for Yb^{3+} and Cr^{3+} ions) are very close to the experimental exchange parameters $J_z=-5.16\ cm^{-1}$ and $J_\perp=+4.19\ cm^{-1}$.[26] This indicates that the kinetic exchange theory is an adequate approach to the description of exchange interactions between lanthanide and transition metal ions in nonmetallic compounds, which can account for both the absolute value of the exchange parameters and the degree of the $4f$-$3d$ exchange anisotropy.

Contributions to the exchange parameters from numerous individual state of the $4f^{12}$-$3d^4$ and $4f^{14}$-$3d^2$ CT configurations have been analyzed in detail and important regularities have been established. In particular, $4f\rightarrow 3d$ and $4f\leftarrow 3d$ electron transfers give rise to a quite different types of the exchange anisotropy: the contribution from the $4f^{12}$-$3d^4$ CT configuration corresponds to an almost pure ferromagnetic XY spin Hamiltonian, while the contribution from the $4f^{14}$-$3d^2$ CT configuration results in an almost pure Ising-like antiferromagnetic Hamiltonian.

Our analysis shows that there is a complicated interplay between numerous contributions to the exchange parameters from individual CT states, which cannot be rationalized in a simple way. The sign of these contributions is different, and the absolute value of separate contributions can be even larger than the net exchange parameters. Not only low-lying CT states, but many CT states lying well above the CT energy gap contribute to the exchange parameters. This is especially true for the CT states involving high-lying levels of the $4f^{12}$ configuration of the ytterbium ion. As a result, the total balance of contributions is very sensitive to the actual CT energies; this implies that the use of a constant average energy U for all CT state is a poor approximation for $4f$-$3d$ exchange pairs.

Symmetry-related selection rules for nonzero contributions from individual CT states have been established for the $YbCrBr_9^{3-}$ dimer of C_{3v} symmetry, which are very helpful in rationalizing the sign and the symmetry of separate contributions. In particular, they account for why the Yb^{3+}-Cr^{3+} exchange spin Hamiltonian is strictly bilinear with respect to the spin $S=\frac{3}{2}$ of Cr^{3+}.

There is a special situation occur in mixed $4f$-$3d$ exchange-coupled pairs due to the fact that the total spin of the lanthanide ion is not a good quantum number. A special care should be taken to bring into correspondence the signs of projection of the effective spin on the $4f$ ion and that of the true spin on the $3d$ ion. When the quantization axis has a rotational symmetry, the sign of the components of the effective spin $S=\frac{1}{2}$ should be chosen according to their transfor-

mational properties, not according to the sign of the projection of the magnetic momentum. This implies that the magnetic momentum of the lanthanide ion may be antiparallel to its effective spin. In this case, the Kramers doublet has a negative g-factor and the sign of the exchange parameters at spin operators should be reversed. This takes place for the $YbCrBr_9^{3-}$ dimer, in which the g tensor of ground Γ_6 doublet of the Yb^{3+} ion is negative.

An important result of this study is that the exchange anisotropy is not necessarily related to the crystal-field anisotropy of the lanthanide ion. Indeed, a very strong $4f$-$3d$ exchange anisotropy is found in the $YbCrBr_9^{3-}$ dimer despite the fact that there is no crystal-field anisotropy on ytterbium ion in the regular $YbBr_6^{3-}$ octahedron.

The superexchange theory developed in this paper is not limited to Kramers ions only, since it can easily be extended (directly or with some minor changes) to other f ions. There are some important cases of other ground CF states, such as the case of the close proximity of a first excited doublet or the case of the Γ_8 quartet occurring for some ions with the odd number of f electrons in cubic crystals. These situations are described by an effective spin $S=\frac{3}{2}$ on the lanthanide or actinide ion (for two close doublets some zero-field splitting should be added). For the even numbers of f electrons the ground Γ_5 triplet can also occur an a cubic crystal field, corresponding to an effective spin $S=1$. In these cases, the superexchange mechanism can be treated quite similarly: the effective exchange Hamiltonian H_{eff} is described by the set of the $\langle m,M_s|H_{\text{eff}}|m',M_s'\rangle$ matrix elements where m now represents the projection of the effective spin S larger that $\frac{1}{2}$, i.e., $S=\frac{3}{2}$ (two close Kramers doublets or the Γ_8 quartet) or $S=1$ (the Γ_5 triplet). Again, these matrix elements are obtained by the projection of the CT states onto the space of wave functions $|m,M_s\rangle$ of the ground level of the f-d dimer (f-f dimers can also be analyzed in the frame of this approach), as described by Eq. (22). The only difference is that for the case of $S>\frac{1}{2}$ the spin Hamiltonian corresponding to the H_{eff} operator is not necessarily bilinear with respect to the effective spin S of the f ion. For instance, some quadratic ($S=1$) or cubic ($S=\frac{3}{2}$) spin operators can appear in the spin Hamiltonian. However, the correspondence between the set of the $\langle m,M_s|H_{\text{eff}}|m',M_s'\rangle$ matrix elements and the exchange spin Hamiltonian can easily be established. In this way, the pseudodoublet ground state (i.e., two close singlet states) or non-Kramers doublets can also be analyzed. Of course, specific details of the mechanism of the f-d or f-f superexchange interactions for non-Kramers ions can differ from the those for the well-isolated ground Kramers doublet given in Sec. III, but the general idea of the approach remains unaltered.

Our analysis demonstrates the actual degree of the complexity of the superexchange problem for lanthanide ions. The $4f$-$3d$ superexchange is complicated even for a relatively simple Yb^{3+}-Cr^{3+} pair. For lanthanide ions from the middle of the $4f$ series (Dy^{3+},Sm^{3+}) the number of CT states increases dramatically. However, despite a larger size of the task, our approach can directly be applied to any combination of the lanthanide ion with the with well-isolated ground Kramers doublet and transition metal ion because the general calculation procedure remains the same as for the present case of the Yb^{3+}-Cr^{3+} pair.

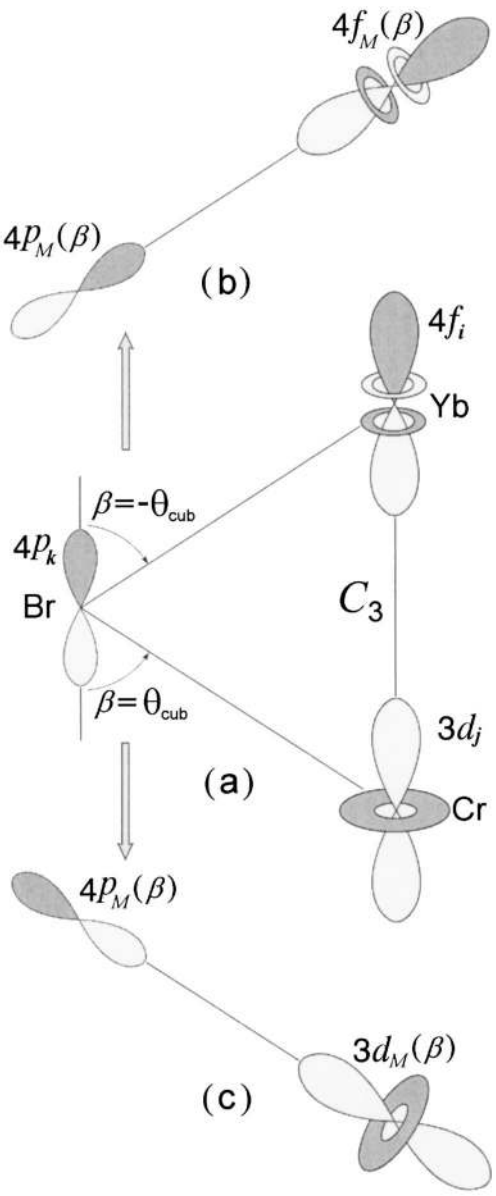

FIG. 6. On the calculation of the A_{ij} quantities. The $4f_i$, np_k, and $3d_j$ orbitals defined in the common quantization axis C_3 are expressed as linear combinations of $4f_M(\beta)$, $3d_M(\beta)$, and $4p_M(\beta)$ orbital defined in the local quantization axes Yb-Br and Cr-Br, Eq. (B3). These orbitals are obtained by rotations of the $4f_i$, np_k, and $3d_j$ orbitals by the angle $\beta=\pm\theta_{\text{cub}}$, which is positive for the Cr-Br local quantization axis and negative for the Yb-Br axis.

ACKNOWLEDGMENTS

Financial support by the Belgian National Science Foundation and Belgian Government under the concerted action scheme, the Russian Foundation for Basic Research (Grant No. 01-03-32210) and the INTAS Grant 00-00565 are gratefully acknowledged.

APPENDIX A

In this section the matrix elements $\langle \Xi_{kl}(AB;SM_s)|H_{AB}|\Xi_{pq}(A\rightarrow B;S'M')\rangle$ are expressed via the $t(4f_i\text{-}3d_j)$ transfer integrals. For this we expand the single-center wave functions $\Psi_k(4f^N)$, $\Psi_p(4f^{N-1})$, $\Phi_l(3d^M;SM_s)$, and $\Phi_q(3d^{M+1};S'M')$ of the lanthanide and transition metal ions over Slater determinants $\mathrm{Det}(\mathbf{p}_A)$, $\mathrm{Det}(\mathbf{q}_A)$, $\mathrm{Det}(\mathbf{p}_B)$, and $\mathrm{Det}(\mathbf{u}_B)$ correspondingly:

$$\Psi_k(4f^N)=\sum_{\mathbf{p}_A} F_k(\mathbf{p}_A)\mathrm{Det}(\mathbf{p}_A), \tag{A1a}$$

$$\Psi_p(4f^{N-1})=\sum_{\mathbf{q}_A} F_p(\mathbf{q}_A)\mathrm{Det}(\mathbf{q}_A), \tag{A1b}$$

$$\Phi_l(3d^M;SM_s)=\sum_{\mathbf{p}_B} D_l(\mathbf{p}_B;SM_s)\mathrm{Det}(\mathbf{p}_B), \tag{A1c}$$

$$\Phi_q(3d^{M+1};M'S')=\sum_{\mathbf{u}_B} D_q(\mathbf{u}_B;S'M')\mathrm{Det}(\mathbf{u}_B), \tag{A1d}$$

where $F(\mathbf{p}_A)$, $F(\mathbf{q}_A)$, $D(\mathbf{p}_B;SM_s)$, and $D(\mathbf{u}_B;S'M')$ are expansion coefficients, in which the vector indices $\mathbf{p}_A$, $\mathbf{q}_A$, $\mathbf{p}_B$, and $\mathbf{u}_B$ are sets of quantum numbers of $4f$ or $3d$ orbitals involved in the corresponding Slater determinant

$$\mathbf{p}_A=\{(4f_{k_1},\sigma_{k_1}),(4f_{k_2},\sigma_{k_2}),\ldots(4f_{k_N},\sigma_{k_N})\}\rightarrow 4f^N, \tag{A2a}$$

$$\mathbf{q}_A=\{(4f_{m_1},\sigma_{m_1}),(4f_{m_2},\sigma_{m_2}),\ldots(4f_{m_{N-1}},\sigma_{m_{N-1}})\}\rightarrow 4f^{N-1}, \tag{A2b}$$

$$\mathbf{p}_B=\{(3d_{l_1},\sigma_{l_1}),(3d_{l_2},\sigma_{l_2}),\ldots(3d_{l_M},\sigma_{l_M})\}\rightarrow 3d^M, \tag{A2c}$$

$$\mathbf{u}_B=\{(3d_{n_1},\sigma_{n_1}),(3d_{n_2},\sigma_{n_2}),\ldots(3d_{n_{M-1}},\sigma_{n_{M+1}})\}\rightarrow 3d^{M+1}, \tag{A2d}$$

in which $\sigma=\pm\frac{1}{2}$ stands for the spin projection of the corresponding $4f$ and $3d$ orbital. Then the two-center wave functions $\Xi_{kl}(AB;SM_s)$ and $\Xi_{pq}(A\rightarrow B;S'M')$ are written as

$$\Xi_{kl}(AB;SM_s)=\sum_{\mathbf{p}_A}\sum_{\mathbf{p}_B} F_k(\mathbf{p}_A)D_l(\mathbf{p}_B;SM_s)\times\mathrm{Det}(\mathbf{p}_A+\mathbf{p}_B), \tag{A3a}$$

$$\Xi_{pq}(A\rightarrow B;S'M')=\sum_{\mathbf{q}_A}\sum_{\mathbf{u}_B} F_p(\mathbf{q}_A)D_q(\mathbf{u}_B;S'M')\times\mathrm{Det}(\mathbf{q}_A+\mathbf{u}_B), \tag{A3b}$$

where the Slater determinants for the joint $4f+3d$ electronic system are the products of the corresponding single-center determinants $\mathrm{Det}(\mathbf{p}_A+\mathbf{p}_B)=\mathrm{Det}(\mathbf{p}_A)\otimes\mathrm{Det}(\mathbf{p}_B)$ and $\mathrm{Det}(\mathbf{q}_A+\mathbf{u}_B)=\mathrm{Det}(\mathbf{q}_A)\otimes\mathbf{Det}(\mathbf{u}_B)$. Consequently, the matrix elements of the perturbation operator H_{AB} are given by

$$\langle \Xi_{kl}(AB;SM_s)|H_{AB}|\Xi_{pq}(A\rightarrow B;S'M')\rangle=\sum_{\mathbf{p}_A}\sum_{\mathbf{p}_B}\sum_{\mathbf{q}_A}\sum_{\mathbf{u}_B} F_k^*(\mathbf{p}_A)D_l^*(\mathbf{p}_B;SM_s)F_p(\mathbf{q}_A)D_q(\mathbf{u}_B;S'M')\times\langle\mathrm{Det}(\mathbf{p}_A+\mathbf{p}_B)|H_{AB}|\mathrm{Det}(\mathbf{q}_A+\mathbf{u}_B)\rangle. \tag{A4}$$

This multiple sum is calculated due to the applying the Slater rules, according to which the nonzero $\langle\mathrm{Det}(\mathbf{p}_A+\mathbf{p}_B)|H_{AB}|\mathrm{Det}(\mathbf{q}_A+\mathbf{u}_B)\rangle$ matrix elements is simply equal to a transfer integral

$$\langle\mathrm{Det}(\mathbf{p}_A+\mathbf{p}_B)|H_{AB}|\mathrm{Det}(\mathbf{q}_A+\mathbf{u}_B)\rangle = \begin{cases} (-1)^P t_{ij} & \text{if } (\mathbf{p}_A+\mathbf{p}_B) \text{ and } (\mathbf{q}_A+\mathbf{u}_B) \text{ differ from each other by only two orbitals } 4f_i \text{ and } 3d_j \text{ with the same spin projections } \sigma_i=\sigma_j \\ 0 & \text{otherwise,} \end{cases} \tag{A5}$$

where P is the parity of the transposition that brings the extra $3d_j$ orbital into the place of the missed $4f_i$ orbital in going from $(\mathbf{q}_A+\mathbf{u}_B)$ to $(\mathbf{p}_A+\mathbf{p}_B)$. Each matrix element $\langle \Xi_{kl}(AB;SM_s)|H_{AB}|\Xi_{pq}(A\rightarrow B;S'M')\rangle$ is therefore written as a sum of t_{ij} transfer integrals multiplied by the corresponding weight factors involved in Eq. (A4), and similarly for the matrix elements $\langle \Xi_{kl}(AB;SM_s)|H_{AB}|\Xi_{rs}(A\leftarrow B;S'M')\rangle$.

APPENDIX B

In this appendix, we provide details of the calculation of the A_{ij} and B_{ij} quantities defined by Eqs. (30) and (31). The key point of these calculations is to express the $\langle 4f_i|h|\chi_k(L_n)\rangle$ and $\langle\chi_k(L_n)|h|3d_j\rangle$ matrix elements (resonance integrals) between the metal orbitals $(4f_i,3d_j)$ and the ligand orbitals $(4s,4p_k)$ defined in the common coordinate frame with the C_3 quantization axis [Fig. 6(a)] via the $\sigma(fp)$, $\pi(fp)$, $\sigma(dp)$, and $\pi(dp)$ parameters. The *i, j*, and *k* indices are projections of the orbital momentum of the respective orbitals to the common C_3 quantization axis of the $YbCrBr_9^{3-}$ dimer. As indicated in the text, these parameters correspond to the resonance integrals of the σ and π types between the metal and ligand orbitals in the local Yb-Br and

TABLE IX. The expression of the $\langle 4f_i|h|4p_k\rangle$ and $\langle 3d_j|h|4p_k\rangle$ matrix elements via the $\sigma(fp)$, $\pi(fp)$, $\sigma(dp)$, and $\pi(dp)$ parameters.

	$4p_1$	$4p_0$	$4p_{-1}$
$3d_2$	$\frac{\sqrt{2}}{6}\sigma(dp)+\frac{2\sqrt{6}}{9}\pi(dp)$	$\frac{\sqrt{2}}{6}\sigma(dp)-\frac{\sqrt{6}}{9}\pi(dp)$	$-\frac{\sqrt{2}}{6}\sigma(dp)+\frac{\sqrt{6}}{9}\pi(dp)$
$3d_1$	$\frac{1}{3}\sigma(dp)+\frac{\sqrt{3}}{9}\pi(dp)$	$\frac{1}{3}\sigma(dp)+\frac{\sqrt{3}}{9}\pi(dp)$	$-\frac{1}{3}\sigma(dp)+\frac{2\sqrt{3}}{9}\pi(dp)$
$3d_0$	$-\frac{1}{3}\pi(dp)$	$\frac{2}{3}\pi(dp)$	$\frac{1}{3}\pi(dp)$
$3d_{-1}$	$-\frac{1}{3}\sigma(dp)+\frac{2\sqrt{3}}{9}\pi(dp)$	$-\frac{1}{3}\sigma(dp)-\frac{\sqrt{3}}{9}\pi(dp)$	$\frac{1}{3}\sigma(dp)+\frac{\sqrt{3}}{9}\pi(dp)$
$3d_{-2}$	$\frac{\sqrt{2}}{6}\sigma(dp)-\frac{\sqrt{6}}{9}\pi(dp)$	$\frac{\sqrt{2}}{6}\sigma(dp)-\frac{\sqrt{6}}{9}\pi(dp)$	$-\frac{\sqrt{2}}{6}\sigma(dp)-\frac{2\sqrt{6}}{9}\pi(dp)$
$4f_3$	$\frac{\sqrt{10}}{18}\sigma(fp)+\frac{\sqrt{15}}{9}\pi(fp)$	$-\frac{\sqrt{10}}{18}\sigma(fp)+\frac{\sqrt{15}}{18}\pi(fp)$	$-\frac{\sqrt{10}}{18}\sigma(fp)+\frac{\sqrt{15}}{18}\pi(fp)$
$4f_2$	$-\frac{\sqrt{30}}{18}\sigma(fp)-\frac{\sqrt{5}}{6}\pi(fp)$	$\frac{\sqrt{30}}{18}\sigma(fp)$	$\frac{\sqrt{30}}{18}\sigma(fp)-\frac{\sqrt{5}}{6}\pi(fp)$
$4f_1$	$\frac{\sqrt{6}}{18}\sigma(fp)-\frac{1}{6}\pi(fp)$	$-\frac{\sqrt{6}}{18}\sigma(fp)-\frac{1}{2}\pi(fp)$	$-\frac{\sqrt{6}}{18}\sigma(fp)+\frac{1}{3}\pi(fp)$
$4f_0$	$\frac{2}{9}\sigma(fp)+\frac{\sqrt{6}}{18}\pi(fp)$	$-\frac{2}{9}\sigma(fp)+\frac{2\sqrt{6}}{18}\pi(fp)$	$-\frac{2}{9}\sigma(fp)+\frac{\sqrt{6}}{18}\pi(fp)$
$4f_{-1}$	$-\frac{\sqrt{6}}{18}\sigma(fp)+\frac{1}{3}\pi(fp)$	$\frac{\sqrt{6}}{18}\sigma(fp)+\frac{1}{2}\pi(fp)$	$\frac{\sqrt{6}}{18}\sigma(fp)-\frac{1}{6}\pi(fp)$
$4f_{-2}$	$-\frac{\sqrt{30}}{18}\sigma(fp)+\frac{\sqrt{5}}{6}\pi(fp)$	$\frac{\sqrt{30}}{18}\sigma(fp)$	$\frac{\sqrt{30}}{18}\sigma(fp)+\frac{\sqrt{5}}{6}\pi(fp)$
$4f_{-3}$	$-\frac{\sqrt{10}}{18}\sigma(fp)+\frac{\sqrt{15}}{18}\pi(fp)$	$\frac{\sqrt{10}}{18}\sigma(fp)-\frac{\sqrt{15}}{18}\pi(fp)$	$\frac{\sqrt{10}}{18}\sigma(fp)+\frac{\sqrt{15}}{9}\pi(fp)$

Cr-Br axes, $\sigma(fp)=\langle 4f_0|h|4p_0\rangle$, $\pi(fp)=\langle 4f_{\pm 1}|h|4p_{\pm 1}\rangle$, $\sigma(dp)=\langle 3d_0|h|4p_0\rangle$, $\pi(dp)=\langle 3d_{\pm 1}|h|4p_{\pm 1}\rangle$, $\sigma(fp)=\langle 4f_0|h|4p_0\rangle$, and $\sigma(fp)=\langle 4f_0|h|4p_0\rangle$. Consider the A_{ij} quantities, Eq. (25)

$$A_{ij}=\sum_{n=1,2,3}\sum_{k=0,\pm 1}\langle 4f_i|h|4p_k(L_n)\rangle\langle 4p_k(L_n)|h|3d_j\rangle.$$

For the C_{3v} symmetry of the $YbCrBr_9^{3-}$ dimer, the nonzero A_{ij} quantities obey the selection rule $i=j$ and $i=j\pm 3$. Indeed, since the $L_{1,2,3}$ bridging bromine ligands transfer to each other upon rotations by the angles $\pm 2\pi/3$, the products $\langle 4f_i|h|4p_k(L_n)\rangle\langle 4p_k(L_n)|h|3d_j\rangle$ for different ligands L_n are related to each other by the phase factor $e^{\pm i(2\pi/3)\Delta m}$

$$\langle 4f_i|h|4p_k(L_2)\rangle\langle 4p_k(L_2|h|3d_j)\rangle = e^{-i(2\pi/3)\Delta m}\langle 4f_i|h|4p_k(L_1)\rangle\langle 4p_k(L_1)|h|3d_j\rangle, \quad \text{(B1a)}$$

$$\langle 4f_i|h|4p_k(L_3)\rangle\langle 4p_k(L_3)|h|3d_j\rangle = e^{i(2\pi/3)\Delta m}\langle 4f_i|h|4p_k(L_1)\rangle\langle 4p_k(L_1)|h|3d_j\rangle, \quad \text{(B1b)}$$

where $\Delta m=i-j$. Therefore, the sum over the ligands ($n=1,2,3$) in Eq. (25) is proportional to the factor

$$1+e^{i(2\pi/3)\Delta m}+e^{-i(2\pi/3)\Delta m}=1+2\cos\left(\frac{2\pi}{3}\Delta m\right), \quad \text{(B2)}$$

which is equal to 3 if $\Delta m=0$ or ± 3 and is zero otherwise.

We express the $\langle 4f_i|h|4p_k(L_n)\rangle$ and $\langle 4p_k(L_n)|h|3d_j\rangle$ matrix elements for a given Br bridging ligand L_n via the $\sigma(fp)$, $\pi(fp)$, $\sigma(dp)$, and $\pi(dp)$ parameters (for concreteness, we consider the ligand L_n with $n=1$). The geometry of the Yb-Br-Cr bridging group in the $YbCrBr_9^{3-}$ idealized dimer is shown in Fig. 6(a). The Cr-Br and Yb-Br bonds make the angle $\beta=\pm\theta_{cub}$ with the C_3 quantization axis,

where θ_{cub} is so called cubic angle, $\cos\theta_{cub}=1/\sqrt{3}$ ($\theta_{cub}=54.7°$).

The $4f_i$, $3d_j$, and $4p_k$ orbitals defined for the common coordination frame can be expanded over the $4f_M(\beta)$, $3d_M(\beta)$, and $4p_M(\beta)$ orbital defined in the local quantization axes Yb-Br and Cr-Br (Fig. 6)

$$4f_i=\sum_{M=3}^{-3} d^3_{Mi}(\beta)4f_M(\beta), \tag{B3a}$$

$$3d_j=\sum_{M=2}^{-2} d^2_{Mj}(\beta)3d_M(\beta), \tag{B3b}$$

$$4p_k=\sum_{M=1}^{-1} d^1_{Mk}(\beta)4p_M(\beta), \tag{B3c}$$

where $d^J_{MM'}(\beta)=D^J_{MM'}(0,\beta,0)$ is the Wigner D function for the momentum J (here $J=3$, 2, 1 and $M'=i$, j, k for the $4f$, $3d$, and $4p$ orbitals, respectively).[51] The $4f_M(\beta)$, $3d_M(\beta)$, and $4p_M(\beta)$ orbitals are obtained from the rotations of $4f_i$, $3d_j$, and $4p_k$ orbitals by the angle β, which is negative ($\beta=-\theta_{cub}$) for the Yb-Br axis [Fig. 6(b)] and positive ($\beta=\theta_{cub}$) for the Cr-Br axis [Fig. 6(c)]. Since in the local quantization axes the nonzero matrix elements $\langle 4f_M(\beta)|h|4p_{M'}(\beta)\rangle$ and $\langle 3d_M(\beta)|h|4p_{M'}(\beta)\rangle$ occur if only $M=M'$, i.e.,

$$\langle 4f_0(\beta)|h|4p_0(\beta)\rangle=\sigma(fp), \tag{B4a}$$

$$\langle 4f_{\pm1}(\beta)|h|4p_{\pm1}(\beta)\rangle=\pi(fp), \tag{B4b}$$

$$\langle 3d_0(\beta)|h|4p_0(\beta)\rangle=\sigma(dp), \tag{B4c}$$

$$\langle 3d_{\pm1}(\beta)|h|4p_{\pm1}(\beta)\rangle=\pi(dp), \tag{B4d}$$

we have

$$\langle 4f_i|h|4p_k\rangle=\sum_{M=1}^{-1} d^3_{Mi}(\beta)d^1_{Mk}(\beta)\langle 4f_M(\beta)|h|4p_M(\beta)\rangle, \tag{B5a}$$

$$\langle 3d_j|h|4p_k\rangle=\sum_{M=1}^{-1} d^2_{Mj}(\beta)d^1_{Mk}(\beta)\langle 3d_M(\beta)|h|4p_M(\beta)\rangle \tag{B5b}$$

or

$$\langle 4f_i|h|4p_k\rangle=d^3_{0i}(\beta)d^1_{0k}(\beta)\sigma(fp)+[d^3_{-1i}(\beta)d^1_{-1k}(\beta)+d^3_{1i}(\beta)d^1_{1k}(\beta)]\pi(fp), \tag{B6a}$$

$$\langle 3d_j|h|4p_k\rangle=d^2_{0j}(\beta)d^1_{0k}(\beta)\sigma(dp)+[d^2_{-1j}(\beta)d^1_{-1k}(\beta)+d^2_{1j}(\beta)d^1_{1k}(\beta)]\pi(dp). \tag{B6b}$$

The coefficients at the $\sigma(fp)$, $\pi(fp)$, $\sigma(dp)$, and $\pi(dp)$ parameters are given in Table IX. Then, according to Eq. (25), multiplying the $\langle 4f_i|h|4p_k\rangle$ and $\langle 3d_j|h|4p_k\rangle$ matrix elements and summing the products over $k=0$, ±1 and three ligands $n=1-3$ [the sum over ligands is simply reduced to the multiplication by the factor defined in Eq. (B2)], we obtain the A_{ij} quantities presented in Table II.

Calculations of the B_{ij} quantities for $4s$(Br) orbitals are performed similarly. Note that in this case only σ overlap between metal orbitals and $4s$ bromine orbitals occurs (Table II).

*Corresponding author. Present address: Department of Chemistry, Katholieke Universiteit Leuven, Celestijnenlaan 200F, B-3001 Leuven, Belgium. Email address: mirsa@icp.ac.ru, vladimir@bohr.quantchem.kuleuven.ac.be (present).

[1] Y. Shimakawa, Y. Kubo, and T. Manako, Nature (London) **379**, 55 (1996); M. A. Subramanian, B. H. Toby, A. P. Ramirez, W. J. Marshall, A. W. Sleight, and G. H. Kwei, Science **273**, 81 (1996).

[2] A. Furrer, P. Allenspach, J. Mesot, and U. Staub, Physica C **168**, 609 (1990); V. Nekvasil, S. Jandl, M. Cardona, M. Divis, and A. A. Nugroho, J. Alloys Compd. **323–324**, 549 (2001).

[3] S. Jandl, P. Richard, M. Poirier, V. Nekvasil, A. A. Nugroho, A. A. Menovsky, D. I. Zhigunov, S. N. Barilo, and S. V. Shiryaev, Phys. Rev. B **61**, 12 882 (2000); V. Nekvasil, S. Jandl, M. Cardona, M. Divis, and A. A. Nugroho, J. Alloys Compd. **323–324**, 549 (2001).

[4] F. Bartolome, J. Bartolome, M. Castro, and J. J. Melero, Phys. Rev. B **62**, 1058 (2000).

[5] S. Quezel, F. Tcheou, J. Rossat-Mignod, G. Quezel, and E. Roudaut, Physica B & C **86–88B**, 916 (1977).

[6] J. Bartolome, E. Palacios, M. D. Kuz'min, F. Bartolome, I. Sosnowska, R. Przenioslo, R. Sonntag, and M. M. Lukina, Phys. Rev. B **55**, 11 432 (1997).

[7] Y. Yamaguchi and T. Sakuraba, J. Phys. Chem. B **41**, 327 (1980).

[8] J. Romero de Paz, J. L. Martýnez, and R. Saez Puche, J. Alloys Compd. **303–304**, 293 (2000).

[9] M. J. P. Gingras, B. C. den Hertog, M. Faucher, J. S. Gardner, S. R. Dunsiger, L. J. Chang, B. D. Gaulin, N. P. Raju, and J. E. Greedan, Phys. Rev. B **62**, 6496 (2000).

[10] S. Hüfner, *Optical Spectra of Transparent Rare Earth Compounds* (Academic, New York, 1978), p. 147.

[11] O. Guillot-Nöel, A. Kahn-Harari, B. Viana, D. Vivien, E. Antic-Fidancev, and P. Porcher, J. Phys.: Condens. Matter **10**, 6491 (1998); O. Guillot-Nöel, V. Mehta, B. Viana, D. Gourier, M. Boukhris, and S. Jandl, Phys. Rev. B **61**, 15 338 (2000).

[12] J. A. Griffin, M. Huster, and R. J. Folweiler, Phys. Rev. B **22**, 4370 (1980).

[13] G. Amoretti, A. Blaise, R. Caciuffo, J. M. Fournier, M. T. Hutchings, R. Osborn, and A. D. Taylor, Phys. Rev. B **40**, 1856 (1989).

[14] V. A. Pashchenko, A. G. M. Jansen, M. I. Kobets, E. N. Khats'ko, and P. Wyder, Phys. Rev. B **62**, 1197 (2000).

[15] M. T. Borowiec, V. Dyakonov, A. Prokhorov, and H. Szymczak, Phys. Rev. B **62**, 5834 (2000).

[16] P. M. Levy, Phys. Rev. **177**, 509 (1969); P. M. Levy, in *Magnetic Oxides*, edited by D. J. Craik (Wiley, New York, 1975), Pt. I, p. 181; M. I. Bradbury and D. J. Newman, J. Phys. Chem. Solids **32**, 627 (1971).

[17] W. P. Wolf, J. Phys. (Paris) **32**, C1-26 (1971).
[18] K. W. H. Stewens, J. Phys. C **5**, 1360 (1972); K. W. H. Stewens, Phys. Lett., C **24**, 1 (1976).
[19] V. S. Mironov, J. Phys.: Condens. Matter **8**, 10 551 (1996).
[20] I. J. Dzyaloshinskii, Phys. Chem. Solids **4**, 241 (1958); T. Moriya, Phys. Rev. Lett. **4**, 228 (1960); Phys. Rev. **120**, 91 (1960).
[21] H. U. Güdel, in *Molecular Magnetism*, edited by E. Coronado *et al.* (Kluwer Academic, Dordrecht, 1996), p. 229.
[22] P. J. McCarthy and H. U. Güdel, Coord. Chem. Rev. **88**, 69 (1988).
[23] A. Furrer, H. U. Güdel, H. Blank, and Heidemann, Phys. Rev. Lett. **62**, 210 (1989).
[24] A. Furrer, H. U. Güdel, E. R. Krausz, and H. Blank, Phys. Rev. Lett. **64**, 68 (1990).
[25] H. U. Güdel, A. Furrer, and H. Blank, Inorg. Chem. **29**, 4081 (1990).
[26] M. A. Aebersold, H. U. Güdel, A. Hauser, A. Furrer, H. Blank, and R. Kahn, Phys. Rev. B **48**, 12 723 (1993).
[27] M. A. Aebersold, H. U. Güdel, A. Furrer, and H. Blank, Inorg. Chem. **33**, 1133 (1994).
[28] P. Allenspach, A. Furrer, H. U. Güdel, N. Furer, and H. Büttner, Physica B **234–236**, 744 (1997).
[29] D. Schaniel, P. Allenspach, A. Furrer, K. Krämer, and H. U. Güdel, J. Alloys Compd. **323–324**, 481 (2001).
[30] P. W. Anderson, Phys. Rev. **115**, 2 (1959); P. W. Anderson, in *Magnetism I*, edited by G. T. Rado and H. Suhl (Academic Press, New York, 1963).
[31] G. J. Wessel and D. J. W. Ijdo, Acta Crystallogr. **10**, 466 (1957).
[32] G. Meyer and A. Schönemund, Mater. Res. Bull. **15**, 89 (1980).
[33] B. Leuenberger, A. Stebler, H. U. Güdel, A. Furrer, R. Feile, and J. K. Kjems, Phys. Rev. B **30**, 6300 (1984).
[34] A. Ceulemans, L. F. Chibotaru, G. A. Heylen, K. Pierloot, and L. G. Vanquickenborne, Coord. Chem. Rev. **100**, 787 (2000).
[35] V. S. Mironov (unpublished).
[36] B. G. Wybourne, *Spectroscopic Properties of Rare Earths* (Interscience, New York, 1965).
[37] C. A. Morrison and R. P. Leavitt, in *Handbook on the Physics and Chemistry of Rare Earths*, edited by K. A. Gschneidner, Jr. and L. Eyring (North-Holland, Amsterdam, 1982), Vol. 5, Chap. 46.
[38] C. Görller-Walrand and K. Binnemans, in *Handbook on the Physics and Chemistry of Rare Earths*, edited by K. A. Gschneidner, Jr. and L. Eyring (North-Holland, Amsterdam, 1996), Vol. 23, Chap. 155, p. 121.
[39] S. Sugano, Y. Tanabe, and H. Kamimura, *Multiplets of Transition Metal Ions in Crystals* (Academic Press, New York, 1970).
[40] A. B. P. Lever, *Inorganic Electronic Spectroscopy*, 2nd ed. (Elsevier, Amsterdam, 1984).
[41] W. T. Carnall, P. R. Fields, and K. Rajnak, J. Chem. Phys. **49**, 4412 (1968).
[42] M. P. Hehlen and H. U. Güdel, J. Chem. Phys. **98**, 1768 (1993).
[43] J. Emsley, *The Elements* (Clarendon Press, Oxford, 1991).
[44] M. Wolfsberg and L. Helmholz, J. Chem. Phys. **20**, 827 (1952).
[45] M. Synek and L. Corsiglia, J. Chem. Phys. **48**, 3121 (1968).
[46] S. Shaik, R. Hoffmann, C. R. Fisel, and R. H. Summerville, J. Am. Chem. Soc. **102**, 4555 (1980).
[47] P. Alemany and R. Hoffmann, J. Am. Chem. Soc. **115**, 8290 (1993).
[48] J. P. Declaux, At. Data Nucl. Data Tables **12**, 311 (1973).
[49] A. D. McLean and R. S. McLean, At. Data Nucl. Data Tables **26**, 197 (1981).
[50] L. L. Lohr and P. Pyykko, Chem. Phys. Lett. **62**, 333 (1979); P. Pyykko and L. Laaksonen, J. Phys. Chem. **88**, 4892 (1984).
[51] D. A. Varshalovich, A. N. Moskalev, and V. K. Khersonskii, *Quantum Theory of Angular Momentum* (World Scientific, Singapore, 1988).